MICROSTRUCTURAL INFLUENCE ON HYDROGEN ABSORPTION IN STEELS

A Thesis

by

MICHAEL ALEXANDER LIU

Submitted to the Office of Graduate and Professional Studies of
Texas A&M University
in partial fulfillment of the requirements for the degree of

MASTER OF SCIENCE

Chair of Committee,	Ankit Srivastava
Co-Chair of Committee,	Homero Castaneda-Lopez
Committee Member,	Matthew Pharr
Head of Department,	Ibrahim Karaman

December 2017

Major Subject: Materials Science and Engineering

ABSTRACT

The presence of hydrogen in structural metals and alloys especially steels has proven to be a problem warranting a significant amount of attention for over a century. In steels presence of hydrogen severely degrades its mechanical properties such as ductility and fracture toughness, commonly known as hydrogen embrittlement. Hydrogen can be introduced into materials during processing or in-service application under aggressive environments. Hydrogen embrittlement is of particular concern under hydrogen rich aqueous environments. Electrochemical charging environments have been shown to have a more deleterious effect on mechanical properties of steels than gaseous environments. For a given environment the ingress of hydrogen into a material is also influenced by its microstructural features. Following this, in this thesis, a comprehensive analyses of the effect of microstructural features on hydrogen absorption in steels have been carried. The focus is confined to pure iron, AISI 1018 low-carbon steel and AISI 4340 high strength alloy steel. The hydrogen is introduced into cylindrical billets of the three materials through electrochemical charging. The total hydrogen content of the charged billets are then quantified following gas fusion analysis principle commonly termed as melt extraction. This allows the quantification of absorbed hydrogen in a given material as a function of charging time. The results reveal that hydrogen content in pure iron increases with charging time and tends to saturate. On the other hand in 1018 and 4340 following initial saturation, the hydrogen content tends to increase again with continued charging. The mechanical properties of the hydrogen charged billets of the three materials are also characterized using nanoindentation technique. Lastly, thermo-kinetic modeling of hydrogen absorption in these materials has been carried out. The modeling results aid in better understating the correlations between hydrogen absorption and microstructural trapping sites present in these materials.

DEDICATION

To my mother and father for all of their support and patience through the years.

To my brother for teaching me the power of learning through teaching.

To my friends Danny, Khris, George, Gerard, Derek, Jason for all the laughs and great times we have all had over the years. Your undying loyalty and general demeanor have gotten me through many times through the years.

To the High Society for supporting me throughout my Texas A&M career. The Wolf Pack will always live on.

To my friends Eric and Bryan, who are some of the best friends you could ever have.

To my brothers of the past, especially Templeton, Nick, Baljot, Brainard, Geo, Nico, Rob, Spencer, Josh, John, Kevin, Ian C, Ian M, and Lorenzo. Thank you for your support and lessons you taught me.

To my friend, Vincent for your drive to push for more.

To my friends Elizabeth, Jessica-Lynn, Christina, and Stephanie for being my friends all these years and always giving me a trustworthy person to come back to.

To my friend, Israel for teaching me much during our time together. I loved the laughs we shared and the time we took to work together. I wish you all the best.

To all of my mentors who were gracious enough to provide me with the strength to develop myself and the fortitude to always forge on, may you always be remembered in my heart and everything that I do.

To all my friends in the Materials Science and Engineering Department for your support and love.

To all those willing to put their lives on the line for the things they love and for the sake of others.

To anybody who I ever knew and loved.

ACKNOWLEDGEMENTS

To all those that helped me during this time, I would like to thank the Materials Characterization Facility at Texas A&M University, specifically Dr. Andrew Mott for teaching me how to polish samples and generally being a helpful individual to my analyses and work, Dr. Winson Kuo for teaching me how to use the Tescan Fera Scanning Electron Microscope, Dr. Wilson Serem for teaching me how to perform nanoindentation, the Microscopy and Imaging Center at Texas A&M University, specifically, Tom Stephens for teaching me a variety of things related to microscopy and sample preparation.

CONTRIBUTORS AND FUNDING SOURCES

Contributors

This work was supported by a thesis committee consisting of Professor Ankit Srivastava and Professor Homero Castaneda of the Department of Materials Science and Engineering and Professor Matthew Pharr of the Department of Mechanical Engineering.

All other work conducted for the thesis was completed by the student independently.

Funding Source

The work reported in this thesis was supported by Texas A&M Engineering Experimentation Station (TEES) through the start-up funds provided to Professor Ankit Srivastava.

TABLE OF CONTENTS

Page

LIST OF FIGURES

LIST OF TABLES

I. INTRODUCTION

The presence of hydrogen in steel has proven to be a problem warranting a significant amount of attention for over a century. From the original work, which began the initial discussion regarding the degenerative properties of hydrogen in steel, by Johnson [1], a plethora of studies have focused on quantifying the role of hydrogen and its relationship with ferritic microstructures. Henceforth, hydrogen is severely degradative when introduced to steels by reducing an array of mechanical properties including ductility, fracture strength, and fracture toughness of steels [2]. The totality of these types of effects is summarily known as hydrogen embrittlement and occurs most probably when hydrogen begins diffusing through the crystal lattice of ferritic steels.

Hydrogen can be introduced to a material through a variety of sources such as during thermal processing, acid pickling, and electroplating processes which each promote hydrogen accumulation in steel. Exposed surfaces that encounter hydrogen first experience a breakdown of diatomic hydrogen before individual atoms are able to penetrate past the initial surface layers whereby the disastrous effects of hydrogen diffusion are experienced. Service conditions that steel structures are used in like those of water electrolysis or certain power applications can also prove to be circumstances that incite hydrogen based failure [3]. The presence of hydrogen is a problem for low carbon steels, which are a common choice as pressure vessels and storage containers for petrochemical and other fuel industry applications [4]. Moreover, the challenge of meeting a growing market for alternative fuel sources has pushed the continued improvement of hydrogen-based fuel cells. As an abundant and environmentally friendly energy source, hydrogen only suffers from the drawback of safe storage and large scale transportation. High strength ferritic steels have been chosen as a material that could be used for hydrogen pipelines, pressure vessels, and compressors while reducing costs of manufacture.

Although hydrogen embrittlement can be a concern even without a continuous source, hydrogen-rich aqueous environments pose a particular problem for steel structures. Electrochemical charging environments are shown to have a more profound effect on diminishing mechanical properties of steels than gas charging environments in shorter

time intervals corroborating that liquid mediums pose an immediate problem to exposed components. In an aqueous environment, a hydrogen reduction reaction which generates hydrogen occurs on the steel surface after prolonged exposure. The ensuing diffusion into the metal causes embrittlement and subsequently premature fracture. For example, the fatigue life of bearing steels can be reduced by a factor of 100 by only a few parts per million of hydrogen residing in their lattice [5]. Moreover, hydrogen assisted cracking (HAC) probability scales upward with the strength level of high strength steels. As these deformation resistant steels are employed more often for applications such as energy storage containers specifically containing hydrogen, it is practical to study the distribution patterns of hydrogen as it pertains to probability of failure. Some failure features of hydrogen embrittlement of steels can manifest as: surface blistering; hydrogen-induced cracking (HIC); hydrogen-induced stress-corrosion cracking (HISCC); hydrogen enhanced and strain-induced vacancies (HESIV) classical, weld, and stress cracking and hydrogen-environment embrittlement (HEE) [6].

The ingress of hydrogen can be influenced by a variety of factors as it moves through a steel microstructure. Trapping sites have been proven to have a strong effect on the diffusivity of hydrogen due to the energy barrier that hydrogen must overcome in order to continue its path through the lattice. These traps include vacancies, grain boundaries, dislocation cores, precipitates, and interphase boundaries. Trapping sites can be distinguished between being shallow or deep. Shallow traps are henceforth referred as sites which possess smaller energy barriers that bind hydrogen. Deep traps are sites that possess a much higher binding energy. A close relationship exists between trapping states of hydrogen in metals and hydrogen embrittlement [7]. Grain boundaries, specifically, can operate as sources and sinks for hydrogen atoms and ions wherein a critical concentration can lead to hydrogen embrittlement. The distribution of hydrogen across a microstructure can also locally affect the mechanical properties of a steel structure leading to premature failure. A distribution equilibrium exists between trap and lattice sites when considering shallow traps. For deep traps, which are saturated at low chemical activities, hydrogen is immobile at ambient temperature. The temperature of application for the steel is also an

important concern as its variability has been proven to affect the diffusion of atoms through a structure [8].

The microstructure of a material can also vastly affect its susceptibility to the influence of hydrogen. Generally, Fickian diffusion models predict that body-centered cubic (BCC) structures are prone to embrittlement due to an open structure and accumulation at interstitial sites. As BCC steels experience high magnitudes of hydrogen diffusion, they have been chosen as the focus of this work. There has been some developments toward creating microstructures that can withstand hydrogen rich environments by taking on large amounts of hydrogen without considerable reduction in mechanical properties [9]. Surface treatments that inhibit the adsorption and subsequent dissociation of hydrogen at a sample surface are another avenue that is being developed as a preventative measure to obstruct hydrogen diffusion. In order to better prepare for the effects of hydrogen upon steel, a study in the diffusion of hydrogen and subsequent distribution in an exposed material is required to properly assess the conditions leading up to hydrogen embrittlement.

To offer a comprehensive analysis of hydrogen absorption and movement in BCC steels, two dual phase steels were chosen. AISI 4340, a high strength low alloy steel (HSLA), features a primarily ferrite-pearlite microstructure that was determined to offer insight into the hydrogen diffusion dynamics in the materials with a large amount of grain boundaries. AISI 1018 is a general purpose, low carbon steel which also features a ferrite-pearlite microstructure, however, its higher percentage of ferrite made it an attractive candidate to confirm the role of ferrite in pearlitic steels. To complement the aforementioned outcomes of analysis, pure iron was studied to offer a baseline of behavior as it offered the simplicity of a primarily ferritic microstructure. The work performed here observes the diffusion of hydrogen in ferritic structures through cathodic charging of uniform cylindrical billets of 4340 and 1018 steel and pure iron. Each specimen was charged to obtain a diffusion profile that could better quantify the behavior of hydrogen as it progresses through the material. Once the samples were charged, their hydrogen content was measured by gas fusion analysis technique commonly referred to as melt

extraction. This device affords a simple method of sample preparation and insertion and generates gaseous content determination in parts per million (ppm) with respect to sample weight. To accompany the results of charging, a thermodynamic model of the diffusing hydrogen was generated from previous work primarily based on the original study by Oriani [10]. The data provided by studying the influx of hydrogen in each structure can help quantify the susceptibility of simple and more complex ferrite based microstructures which can be extrapolated to understand more complex dual and multiphase structures with variety of components. This notion is extended towards the modeling work performed complementary to this study which focuses on considerations for microstructural trapping features which previous models do not take into account or do so in a rudimentary manner.

The results of the charging reveal that hydrogen aggregates more within 4340 steel than in 1018 and pure iron due to a larger agglomeration of trapping sites such as grain boundaries, different phases, and cementite precipitates, which are carbide in nature. Although both steels appear to follow a similar initial pattern of hydrogen absorption, the charging of 4340 caused macroscopic degradation to the material at longer charging periods. Furthermore, 4340 hydrogen content tested consistently higher than charged specimens of 1018 and pure iron with the same charging time. In contrast, neither 1018 nor pure iron suffered the macroscopic corrosive effects of continuous hydrogen charging and exposure to an acidic environment within the limits of the experiments carried out in this work. This would imply that 4340 is more susceptible to corrosion due to hydrogen from aqueous environments while hydrogen diffuses through the ferrite dominant microstructure of 1018 and pure iron leading to the lower registered hydrogen content values exhibited by both materials. The thermodynamic hydrogen diffusion model reinforces this result by accurately predicting the amount of total hydrogen in the material with respect to the types of trapping sites existing in the material.

The charging of these iron based materials provides an analysis of the hydrogen diffusion in ferritic microstructures of differing strengths and structural constituents. The measurement of hydrogen and the modeling of the resulting data for each material can

offer a better introspective into the mechanism of hydrogen diffusion and solubility under various exposure times in an aqueous environment. The work performed here further elucidates the interaction behavior between trapping sites and hydrogen in steel microstructures.

II. BACKGROUND AND PREVIOUS WORK

Hydrogen diffusion and absorption through steel microstructures has been observed through a variety of methods over the last couple of decades. Common use devices such as steel pressure vessels are subject to a variable number of loading cycles that may incite premature cracks to form and exacerbate preexisting ones to grow leading to poor mechanical properties. Hydrogen first breaks down at the surface of the exposed device before diffusing into the structure. Lang reported that the atomic size of hydrogen is approximately 0.1 nm [11]. The small atomic size and light weight of hydrogen allow it to be very mobile and highly diffusive in steel over large distances even in ambient conditions [12, 13]. As compared to other elements, hydrogen can be particularly deleterious due to its high mobility [14]. Due to its extremely small atomic radius, hydrogen may be subject to unintentional addition to various metallic structures during manufacturing or corrosion applications [15]. Depover found that hydrogen could diffuse through a sample thickness and thus assist in hydrogen related ductility reduction.

Various reports have indicated that hydrogen diffusion is triggered through a drop of hydrogen chemical potential at stress centers [16-18]. The activation energy of hydrogen is quite low as hydrogen moves through the ferritic lattice as a proton that first occupies interstitial lattice sites before it tunnels through to the bulk of the host material. Hydrogen absorption occurs more often from electrolytes such as those in aqueous media. There are three important reactions that occur during the corrosion of iron in an acid environment [6]:

The Volmer reaction: Anodic dissolution of Fe

$$\mathrm{Fe} + 2\mathrm{H}^{+} = Fe^{2+} + 2H_{ad}$$

The Tafel reaction: Recombination of adsorbed H

$$2H_{ad} = H_2(gas)$$

The Absorption of H_{ad}

$$H_{ad} = H(dissolved)$$

Diffusion of hydrogen in ferritic steels can prove disastrous since hydrogen typically moves immediately to defects among other problem sites. Mobile hydrogen specifically is known to cause damage in ferritic steels [19]. External stresses can also play a role in promoting the movement and accumulation of hydrogen through a steel structure. To begin studying diffusion, it is important to consider how hydrogen is introduced to the material. Figure 1 presents a depiction of potential energy diagrams for different diffusion conditions. While some studies have chosen to emulate service conditions, others have focused on more severe environments in lieu of experiments [20]. The process of imbuing a specimen with hydrogen typically begins with some type of charging procedure. Charging of a material requires a sample to be connected to some sort of power supply to generate a polarity that attracts the hydrogen from the exposure medium. In most hydrogen charging tests, the charging procedure has employed cathodic polarization in order to diminish the agglomeration of any corrosion product which acts as a hydrogen diffusion block.

There are a variety of electrochemical cell types that can be employed to induce hydrogen charging. The most commonly employed types of cell are those of the galvanic two electrode or Devanathan three electrode electrochemical cell [2, 6, 21]. Devised by Luigi Galvani, the electrochemical galvanic cell derives energy from two simultaneous redox reactions that occur within the cell. Hydrogen absorption, permeation and diffusion were first measured in the three electrode configuration using the electrochemical double cell proposed by Devanathan and Stachurski [22]. The iron or steel membrane possesses an entry side acting as the cathode where charging occurs while the exit side is oxidized anodically. The reference electrode is typically a saturated calomel electrode (SCE) that is placed between the cathode and anode. Two types of hydrogen charging are typically applied in these cells: electrolytic charging from an aqueous solution or gas-phase hydrogen charging. Both techniques were employed by Grabke and Riecke to measure at low and high hydrogen activities in pure iron samples. Their work found that enhanced anodic dissolution reaction or slowed recombination reaction can lead to very high hydrogen activities which cause severe absorption of hydrogen. Novak et al. [23] modeled

the effect of hydrogen in AISI 4340 by first diffusing steel into samples by thermal precharge in hydrogen gas. Mobassar et al [24] employed an electrochemical hydrogenation process resembling that of Shim et al [25]. Here, in-situ electrochemical charging of double notched specimens was performed in H_2SO_4 solution.

Other electrochemical charging cell configurations like that of Laureys et al [26] chose to simply use prolonged time periods to ensure uniform charging. Their method employed electrochemical cathodic charging between 2 anodes for two hours which reduced surface defects and internal damage while ensuring full hydrogen saturation. For gaseous hydrogen deposit, Novak et al used a thermal precharge in an autoclave for a two week period to charge the sample with hydrogen gas. This was to ensure proper distribution to hydrogen at sites in the steel sample. The procedure of Nagao et al was similar in methodology but used a longer duration of 21 days. Time of charging has proven to be a significant factor in determining the amount of hydrogen permeates through a sample. Various reports have shown that as time has increased hydrogen either diffuses through the sample or becomes trapped at adsorption preferred sites in the lattice or microstructural features.

Trapping of hydrogen has been proven to affect the diffusivity of hydrogen in steel. Oriani first postulated that microstructure affects the local distribution of H such that an equilibrium exists between H in trapping and in normal interstitial lattice sites [10]. From the trapping model proposed by McNabb and Foster [27], hydrogen atoms move through the lattice in a random manner and tend to be trapped or delayed at so called trapping sites. There are different types of traps in steels with a continuous spectrum of binding energies. In their work, Grabke offered a simple distinction between traps differentiated by binding energy ΔH and β which represents the product of the concentration of hydrogen and the ratio between the rate of reaction versus the number of normal interstitial sites N.

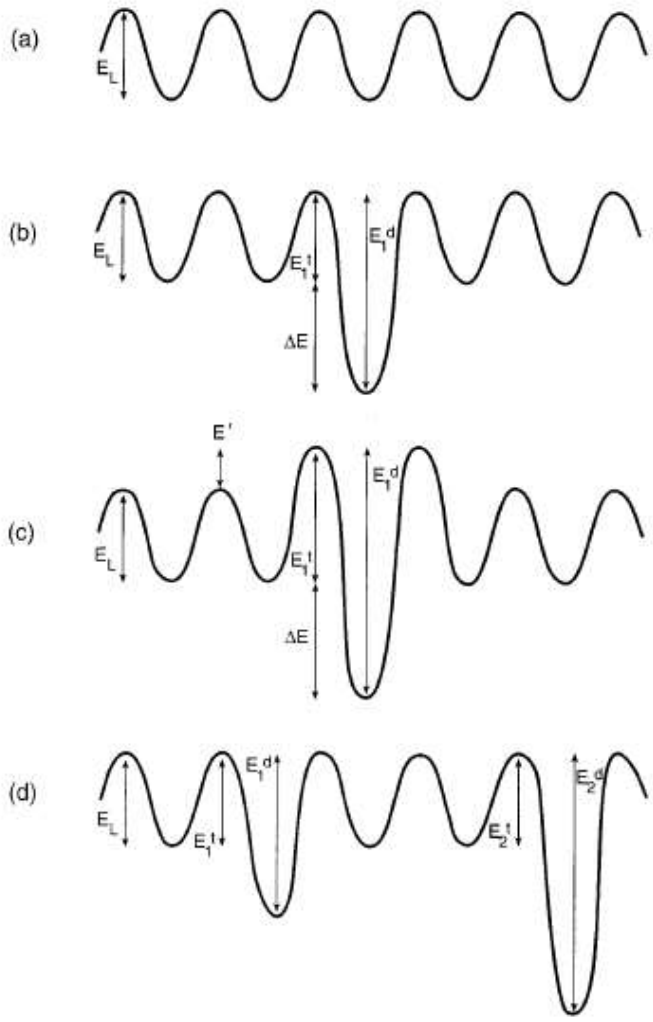

Figure 1: Potential energy diagrams. For (a) lattice diffusion, (b,c) diffusion with a single type of trap (d) diffusion with two types of trap. Reprinted from [28]

The interplay between dislocations in a steel and hydrogen from an environment can also factor into the impedance of hydrogen. Takai reported that edge dislocations with a hydrostatic stress field and hydrogen is larger than interaction with screw dislocations without a hydrostatic stress field for BCC structures. Hydrogen in iron is a mobile interstitial solute atom. Elastic models represent this as a source of elastic distortion that occupies interstitial sites in a BCC lattice [29]. The binding energy between edge

dislocations and hydrogen is reported to be 58 kJ/mol [30]. Hirth calculated the binding energy between screw dislocations and hydrogen to be 19kJ/mol and 20-30 kJ/mol [31]. These values corroborate the results reported by Grabke and show that edge dislocations are the more effectual trapping mechanism between mechanically induced defects. Novak said that a similar energy spectra exists in hydrogen-charged and uncharged 4340 samples. However, trap sites with a binding energy of 18 kJ/mol were related to the elastic strain field of dislocations while sites corresponding to 48 and 72 kJ/mol were associated with interfaces. Trapping in steel has been observed to have beneficial properties as well. The degradation posed by mobile hydrogen can be mitigated if hydrogen becomes trapped. Some work has even proven that engineered hydrogen trapping sites can reduce any deleterious effects of trapped hydrogen [32]. It was suggested by Pressouyre [33] that a homogeneous distribution of strong, innocuous traps could assuage hydrogen embrittlement by reducing the speed at which hydrogen could gather at locations of potential crack initiation. The operational conditions that steel is subjected to can play a role in trapping as well. Low temperatures (< 200 °C) can also promote hydrogen binding to traps at an energy level lower than normal interstitial sites. However, Takai [34] noted that the final fracture stage of embrittlement does not require hydrogen. It was reported that an increasing density of lattice defects introduced by mechanical deformation and weakly trapped diffusive hydrogen is a direct cause of hydrogen embrittlement.

Lattice structures have been shown to have a distinct influence on the behavior of hydrogen ingress in a steel. Body-centered cubic iron base alloys and steels are particularly susceptible to hydrogen embrittlement. These materials typically exhibit very low hydrogen solubility and very high diffusivity of hydrogen in the structure [12]. These materials feature tetrahedral and octahedral interstitial sites where hydrogen can adsorb to the surface and tunnel through. Face-centered cubic materials which are typically stainless steels and nickel base alloys are much less susceptible to hydrogen embrittlement. Evers reported that hydrogen has a preference to act as a solute in austenite. The solution energy of hydrogen depends on the local coordination while possessing a moderate correlation with the actual volume of the interstitial site. Effective centers for hydrogen diffusion can

occur within open structures, FCC grain boundaries, and various different interstitial sites which promote incorporation of hydrogen atoms [35].

There has also been a great deal of work done to study specific microstructural features and compositional effects that influence the diffusive properties of hydrogen. Literature review has shown that microstructure features can determine the susceptibility of a steel to the detrimental effects of hydrogen. Hydrogen tends to segregate at structural defects such as grain boundaries. It has been suggested that segregation of hydrogen controls the material properties of a hydrogen imbued material [12]. Venezuela et al used steel samples consisting primarily of ferrite and martensite. Ab initio calculations based on density functional theory were able to confirm the enhanced solubility of H in austenite grains compared to ferrite grains. This was also corroborated by Han who reported that the diffusion of hydrogen in austenite is many orders of magnitude slower than ferrite at room temperature. These studies have suggested that austenitic steels, specifically stainless steels, are better suited for hydrogen rich environments. Studies on hydrogen diffusion in pearlitic steels found that microstructural orientation of pearlite and non-metallic inclusions affect hydrogen permeation due to the interactions between these inclusions and H [36-38]. Chan measured the diffusivity and permeability of hydrogen through different orientations of a random ferrite pearlite structure versus that of a banded ferrite pearlite microstructure. It was determined that hydrogen could not diffuse as easily through layers of pearlite and ferrite but did find preferable avenues through ferrite-pearlite interfaces and grain boundaries. A random structure was found to have approximately equal values of diffusivity and permeability in each direction measured. Mobbassar determined exposure levels with different maximum hydrogenation times depending on the steel's inherent brittleness and susceptibility to hydrogen embrittlement. Each sample's behavior was correlated with its prior austenite grain sizes and hardness. Hydrogen appears to reduce cohesive strength of prior austenite grain boundaries which results in intergranular fracture at prior austenite grain boundaries [39].

Once hydrogen has penetrated the lattice, it is important to accurately determine the hydrogen content of the lattice to study its effects. Furthermore, due to the small atomic

size of hydrogen, it can be challenging to pinpoint the exact location of hydrogen in the microstructure. To this effect, there are a multitude of studies that utilize a wide array of analysis methods. The electrochemical method of determining hydrogen involves measuring hydrogen oxidation current curves which are proportional to the density of H atoms on a metal surface. This type of measurement takes advantage of the fact that hydrogen exists in metals as individual H-atoms and not as diatomic hydrogen molecules. Cui performed hydrogen content analysis through this method by subjecting a hydrogen charged steel in dilute NaOH solution to a positive electric field in order to diffuse H out from the steel. As H is oxidized at the metal surface, a corresponding H oxidizing current (i_H) is produced. This current is made up of the hydrogen oxidation current and background reference current. A reference current is determined through measurement of an uncharged specimen. Current transients can also help to determine hydrogen activity when the filling and emptying of flat traps is considered [6]. These transients correspond to the absorption of hydrogen into the material during charging and the emptying of traps through anodic oxidation while discharging. The trapping effect could then be quantified by the time it took hydrogen to appear at the exit side after beginning of charging. Thermal desorption analysis (TDA) is a technique that can measure hydrogen uptake. Koyama [40] performed in the range between room temperature to 650K using mass spectrometry to measure the diffusible hydrogen content. TDA was started within 20 min after hydrogen charging to minimize hydrogen outgassing. Hydrogen content is also observable through thermal desorption spectroscopy (TDS). Deep traps saturate during initial charging and trap hydrogen during long-term discharging. Liu and Zhao [3] measured the content of hydrogen in samples and set a temperature limit of 400°C to differentiate between diffusible and non-diffusible. TDS also offered an estimate to the critical hydrogen content of the experimental material.

As the results of the aforementioned studies suggest, hydrogen diffusion can lead to the catastrophic phenomena known as hydrogen embrittlement (HE). This process occurs when hydrogen is introduced to metals such as steel whereupon the ensuing ingress into the steel brittles the structure leading to fracture. The hydrogen embrittlement process

depends on three major factors: the source of hydrogen, the transport that moves atomic hydrogen to regions within the metal to cause embrittlement, and the embrittlement mechanism itself [41]. The diffusion of hydrogen into steel has variety of mechanisms that work to move the particle throughout the microstructure as well as a plethora of consequences may occurs based on hydrogen embrittlement. Movement of singular hydrogen atoms can be stopped by an array of trapping sites that are mostly microstructural features or alloying elements. These traps also exist in a wide range of binding energies that either keep hydrogen or allow its movement through the lattice. The method of imbuing steel with hydrogen is widely varied between each study with no method noted as superior to another. Microstructure and alloying elements can play a significant role in the behavior of mobile hydrogen in a steel microstructure. Coatings can also represent barriers to diffusion and adsorption of hydrogen in a ferritic steel. The measurement of hydrogen content can also be done through a great deal of electrochemical, melt extraction, or mass spectrometry based methods.

III. EXPERIMENTAL METHODOLOGY

The different ferrite based samples were charged by following a procedure that would allow facile transition from the electrochemical cell post charging to the G8 Galileo, device for hydrogen content measurement via melt extraction. This first required creating samples of the proper dimensions to quantify hydrogen penetration into the bulk of each specimen. These dimensions further required a design that could afford immediate analysis by the G8 Galileo due to concerns regarding the quick outgassing of hydrogen. After samples were of proper size, an electrochemical cell featuring a two electrode configuration was assembled. Once samples were charged, they were prepared for hydrogen measurement analysis.

Figure 2: Specimens of (left) 4340 and (right) 1018 steels used for hydrogen charging experiments.

Element	Fe	C	Cr	Mn	Mo	Ni	P	Si	S
Composition	95.09-96.08%	0.38-0.43%	0-0.040%	0.60-0.80%	0.70-0.90%	1.65-2.00%	0.35%	0.20-0.35%	0.040%

Table 1: Composition of 4340 as provided by McMaster-Carr

Element	Fe	C	Mn	P	Si	S
Composition	98.06-99.42%	0.13-0.20%	0.30-0.90%	0.04% Max.	0.15-0.30%	0.50% Max.

Table 2: Composition of 1018 as provided by McMaster-Carr

Element	Fe	Mn	C	P	S
Composition	99.8%	<0.08%	<0.02%	<0.02%	<0.15%

Table 3: Composition of Pure Iron as provided by Goodfellow

Rods of 4340 and 1018 steel were obtained from McMaster-Carr with nominal compositions provided in Table 1 and Table 2, respectively. 2N pure iron rods were obtained from Goodfellow with nominal composition provided in Table 3. Analysis billets were made from all three types of rods. Samples were lathed down from the rods to obtain the proper dimensions for charging and subsequent hydrogen content analysis. Figure 2 presents an image of 4340 and 1018 steel billets. Cylindrical specimens were determined to offer the best solution to both requirements. One of the flat surfaces was chosen as a connection to the electrical wiring required to charge the sample. These cylindrical samples were lathed down from the rods and possessed an equal length and diameter of 6.35 mm [0.25 in x 0.25 in] which allowed for immediate delivery to the hydrogen content analysis instrument, the G8 Galileo. Due to the size of the funnel leading to the heating chamber of the G8 Galileo, specimens were required to be fabricated in such a way to be inserted into the funnel. Furthermore, while typical samples employed in the Galileo are flat circular samples, the thicker cylindrical samples allowed for a look into the development of hydrogen in the material lattice beyond the depth of the surface. Thinner samples could not offer a determination of the effusion of hydrogen into the bulk of a sample which would not encapsulate a larger behavior spectra of the hydrogen storage.

Some tensile testing was performed on round bar specimens to confirm the as received material properties of all three materials from the values provided by the manufacturers. This data was obtained to confirm a correlation between the strength of samples and their susceptibility to hydrogen embrittlement as is mentioned in various work [42]. The results of the tests here indicate that 4340 is the strongest of the three materials studied here with a yield strength of 841 MPa while exhibiting an elongation of 13%. As the material with intermediate mechanical properties, 1018 possesses a yield strength of 372 MPa and an elongation of 23%. As expected, the yield strength of pure iron is the lowest of the three at 131 MPa while also exhibiting the highest ductility.

Correlating the mechanical properties of each material to its respective microstructure is typical practice in metallography as these determinations can provide an in depth understanding of the features at play when a material undergoes a mechanical

response. To observe the microstructure of each sample used in this study, typical sample preparation for the metallography of steel was performed. Each type of sample was initially embedded in bakelite while in billet form. Next, each bakelite puck was ground down on the end where the sample was showing using SiC papers of 600 and 1200 grit. Afterwards, each sample was polished using diamond polish and micron cloths in the order of 9, 6, and 1 um. All three samples were etched with 2% nital solution to uncover microstructural features unable to be observed through polishing alone. This provided the adequate finish for proper topographical analysis of each sample surface.

The microstructures of 4340, 1018, and pure iron were each examined using the Tescan Fera Scanning Electron Microscope through secondary electron and backscatter electron modes to assess the topography and relative amounts of each microstructural phase characteristic of steels. As steels, both 1018 and 4340 feature a topography that possesses regions of heterogeneity which support the mechanical properties of the material given the application. Pure iron, on the other hand, exhibits more homogeneity due to the purity of the material as it features almost entirely ferrite.

III.A Hydrogen Charging Experiment

A series of steps was performed to provide proper charging to the 4340 and 1018 steel and pure iron samples. The steel and pure iron samples were spot welded to a galvanic wire with gauge diameter of 0.7264 mm (0.0286 inch) provided by Malin Company. This diameter and wire type were chosen to create an adequate connection from the sample to the power supply. The wire was fitted through a hollowed glass casing. The casing prevented the metal wire from being subject to additional charging apart from the sample and made the sample the primary conduit for hydrogen absorption from the solution. This configuration made a connection between the power supply and the sample that provided an adequate vehicle for hydrogen storage within the sample microstructure. Further isolation of the wire from the charging solution required the use of an adhesive to bond the top surface of the sample, where the wire had been spot welded, to the bottom of the

tubing that touched the sample. Figure 3 provides a view of the sample-tubing assembly with PWS 1825 power supply.

Previous work by Cui [43] had pointed to polishing the exposed surface area of a sample with very fine grit to ensure proper hydrogen permeation into the bulk of ferritic microstructures featured in both steels and pure iron. Exposed areas of the sample were initially polished using 1200 grit SiC paper in order to remove any adhesive that had run over from the top to the sides or bottom of the sample and to further clean the sample from any contamination that may have occurred during fabrication or handling of the specimen. Once all evidence of the adhesive was removed, each sample was subject to continued polishing until a smooth surface was produced that was free from any post processing effects associated with the fabrication of the samples. All samples were subjected to the same polishing procedure. Pure iron required much less force during polishing due to the softness of the material. Under these conditions, samples were polished as best as possible to remove any products that could potentially affect any results.

Galvanic electrochemical charging cells were assembled by using a 150 mL beaker as the containment cell and a rubber cap that possesses two holes: a hole with a diameter of 6.45mm [+/- 0.02] which is slightly above the outer diameter of the tubing where the glass encased wire could be fitted and a smaller hole in the cap through which a platinum counter electrode connection could be fitted. The counter electrode acted as the cathode from the power supply while the sample assembly acted as the anode. To check the suitability of the platinum counter electrode for use in the procedure, graphene electrodes were cross-referenced against the charging values of the platinum counter electrode. A comparison of the values generated by both counter electrode materials were within reasonable agreement.

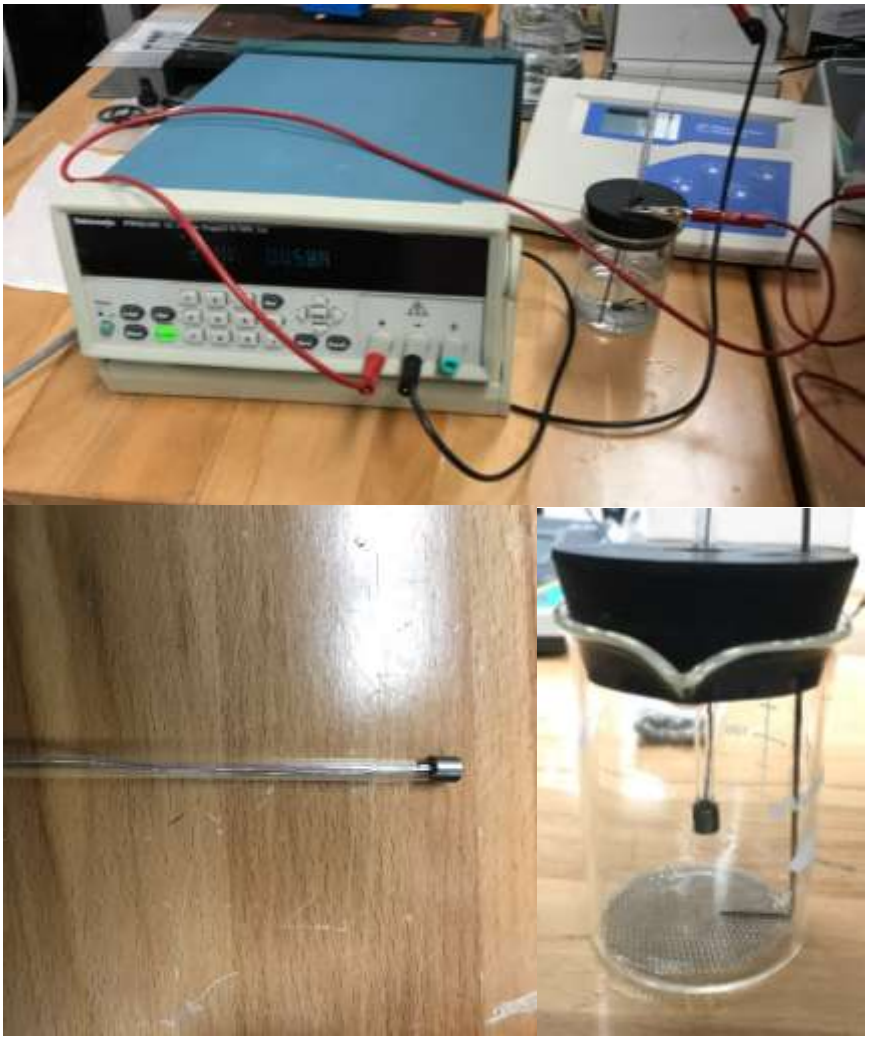

Figure 3: (Top) The electrochemical cell assembly powered by PWS 1825. H_2SO_4 solution fills the beaker to 100 mL ensuring proper submergence of the sample (Left) Sample-tubing assembly with connection made to steel sample. (Right) Electrochemical cell

A PWS 1825 was connected to power the electrochemical charging of the steels and pure iron samples. The PWS was set to constant current operation using voltages ranging from 2.4V to a maximum limit of 3.0V. Depending on how long samples had been charged, these values fluctuated with slight decreases for the steels and steady increases for pure iron. Cathodic charging was performed at room temperature to diminish any temperature based effects on hydrogen diffusivity. The constant current value of 58 mA

was determined through calculation of the necessary power to charge a steel sample that is not in sheet form. Due to the nature of the sample assembly, the exposed area of the sample was the circumferential and bottom area of the cylindrical billet. As the spot welded wire and super glue connections would both require the sample to be ground down so as to not register improper readings, the top surface of the billet where the connections are made is not considered as exposed area. The total exposed area in aqueous solution was 170.44 mm^2. This procedure was similar to the work performed by Cui [43]. Choosing to keep current constant allowed proper hydrogen diffusion for charging times of 0.5, 1, 2, 5, 10, 15, 20, 24, and 30 hours. These times were chosen in order to analyze the evolution of hydrogen to each microstructure and assess the transport phenomena and trapping of hydrogen. This data could provide a diffusion profile for each material to quantify the effect of hydrogen without the influence of deformation.

To charge the steel and pure iron samples, sulfuric acid was used as a part of a charging solution within the electrochemical cell. The strength of the solution was determined to be 0.5M H_2SO_4 from previous work by these procedures [15] [43]. For each liter of solution, 27 mL of sulfuric acid was added to provide the proper solution concentration. Once the charging solution had been prepared, each electrochemical cell was filled with 100 mL of the solution before each charging operation. Three tests were performed for each test time chosen to confirm accuracy of results and create a complete diffusion profile.

III.B Quantifying Hydrogen Content

Hydrogen measurement has proved to be a troublesome necessity to understand the evolution of hydrogen in ferritic microstructures. The hydrogen content of each specimen was determined by a gas fusion analysis method known as hot melt extraction immediately after failure.

For the purposes of this work, there was a necessity to circumvent the time that electrochemical methods take to determine the hydrogen content of a material due to concerns of accuracy and outgassing from the steel samples. As such, it became pragmatic

to employ a quick measurement device. Furthermore, since this study considered two different types of steel and pure iron, a sufficient device of measurement was required. The G8 Galileo is a gas fusion analysis based device that offers a simple method of hydrogen measurement in metallic samples with relatively simple sample preparation. Specifically, the system utilizes a high temperature furnace to melt metallic samples down so that the gaseous contents of the sample can be registered. This reduced the amount of time between cessation of charging and determination of hydrogen content. Thus, the amount of outgassing would be negligible. Measurements of total hydrogen content in steel proved much simpler than the electrochemical methods utilized in these works [6] [21, 24] [43]. For the purposes of this work, the hydrogen content in steel diagnostic option was chosen for the 1018 and 4340 steel samples as well as the pure iron samples. As all three microstructures were primarily ferritic, choosing the diagnostic option to read hydrogen from steel was deemed appropriate for each material.

At the top of the Galileo, samples can be loaded into a funnel that connects to the inner chamber. Upon insertion of a sample, the funnel directs the sample to a connection made within the inner chamber of the Galileo. A graphite crucible is placed on the circular copper platform with a concave ring attachment prior to each operation. Due to the nature of sample destruction, each crucible could only be used once due to the high temperature application and melting of the metal samples.

Before each analysis, the crucible is removed to allow for the inner chamber to be cleaned of any sample residue that may have occurred due to the thermally destructive nature of the analysis. This step is important to ensure no contaminants from any previous experiment could affect the outcome of a current analysis. Hydrogen content of a sample is measured against sample mass provided by scale outfitted to the Galileo software. Samples were first weighed to register a mass from which the software could reference to measure the parts per million (PPM) content of hydrogen. After mass measurement, the interface is prepared to perform hydrogen analysis. When a sample is inserted into the funnel, the stage, where the graphite crucible is placed, rises to the top in order to make a connection with the funnel. This ensures proper sample delivery to the crucible. Once

analysis is chosen a current is generated that heats the crucible to a temperature required to melt the sample completely in a period of 84 seconds. A display of the hydrogen content in parts per million is then generated for review by the computer interface.

III.C Sample Prep for Hydrogen Measurement

Once charging was complete, samples were extracted from the electrochemical cell for hydrogen content analysis. In order to remove the billet from the glass tube assembly, the sample was bathed in acetone to remove the adhesive layer connecting the glass tube to the metal sample. The wire connecting the sample to the power supply was also removed. Any remaining traces of the adhesive that had trapped pieces of the glass tube or metal wire were ground down using water and 320 grit sand paper at a speed of 150 revolutions/minute. The grit paper and revolution speed were chosen specifically to create a smooth top surface in a short period of time to minimize hydrogen outgassing. After a smooth surface was achieved on the top surface of the sample, the cylindrical area and the bottom surface of the sample were cleaned using water and 1000 grit sand paper at a speed of 100 revolutions/minute. This grit and revolution speed was chosen so as to introduce minimal deformation on the exposed sample surface as deformation could result in a measure of outgassing. Cleaning was necessary due to a dark film forming on the exposed portions of the sample that was especially prevalent at charging times after five hours. Longer charging times produced darker films upon the exposed sample surface.

Once the dark film had been removed, samples were first dried to absorb any excess water still on the sample surface. Next, samples were air dried to ensure no residual water was present on the surface as this could produce an incorrect reading. Samples were then individually wrapped in a soft tissue to introduce as little exposure to contaminants as possible before being taken to the G8 Galileo for hydrogen content analysis. After hydrogen content amounts were obtained, the curves generated by the software interface were stored. This data is presented along with all pertinent results in the next section.

IV. RESULTS AND DISCUSSION

A proper understanding of the interplay between microstructural features and hydrogen absorption is necessary to quantify the effects of hydrogen in ferritic microstructures. Olson [44] suggested that control of material composition could help increase the resistance of steel against hydrogen cracking. An analysis of each microstructure is provided to correlate with the hydrogen diffusion profiles generated. A detailed introspective of the diffusion profiles generated during the testing can help point to most prominent factors influencing the movement of hydrogen through the lattice.

IV.A Analysis of Microstructure

In the work performed by Dougherty et al, the microstructure of 1018 steel as received consisted of a fine distribution of ferrite and pearlite grains that slightly banded along the extrusion direction [45]. Figure 4 presents two images from different scales of the 1018 microstructure. The 1018 microstructure as received for the work here appears to possess similar features to the microstructure proposed by the work of Dougherty. However, the pearlite also appears to distribute in island-like agglomerations around the ferritic grains along with the band like configurations. From the SEM micrographs obtained, a reasonable estimate for the ratio between ferrite and pearlite existent in the microstructure would be 60-40, respectively. The ferrite grains in 1018 possess a width of 10-25 μm on average. Pearlite grains possess widths of about 10-20 μm with islands of pearlite on the shorter end of the scale while bands exist on the longer end. This microstructure features only fine pearlite structures. Among the defects present in the material, small voids are apparent in the microstructure. These exist most likely due to the processing method and are unavoidable defects that exist within the microstructure. The voids in 1018 range from about 1-2 μm. While these sites do trap hydrogen, they are not a prevalent feature of the microstructure and most likely do not contribute a great deal toward the amount of hydrogen measured in the analysis.

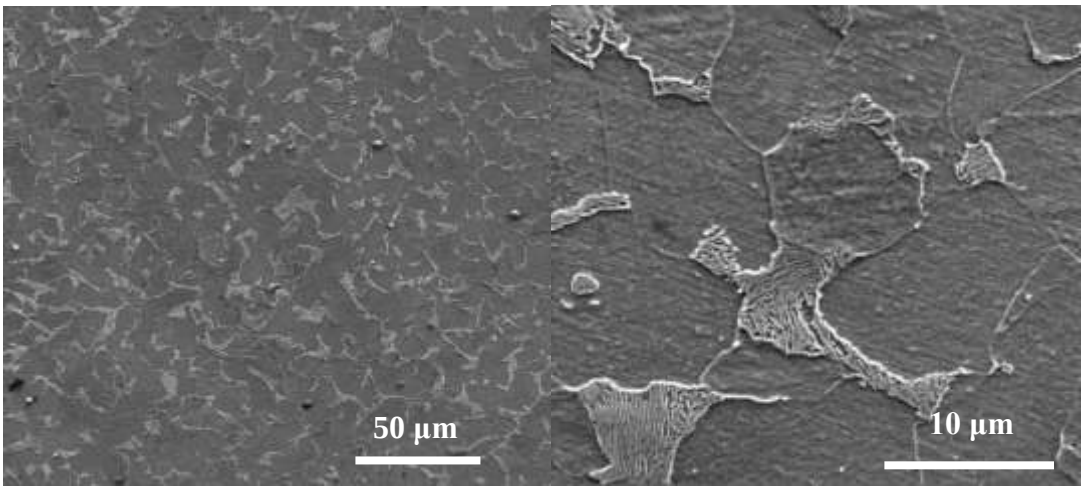

Figure 4: Secondary electron SEM images of 1018 microstructure. (Left) At 50 µm scale and (right) at 10 µm scale.

Figure 5 presents secondary electron SEM images of 4340 with two different scales. 4340 steel similarly possesses ferrite grains but pearlite also exists within the material microstructure. Upon estimation using the electron micrographs, the ratio of ferrite grains to that of pearlite appears to be about 30-70, respectively. Ferrite grains in 4340 range from 10-20 µm in width. The pearlitic grains exist in various configurations with angular offsets between grains and possess a width range of 10-15 µm. The pearlite also occurs in coarse and fine microstructural phases with various grain orientations. This could indicate the susceptibility of 4340 to hydrogen permeation as grain boundaries and microstructure features, where hydrogen can be trapped, constitute a large portion of the 4340 steel. This proposal is affirmed by the work of Danford [46] which proposes that intergranular surfaces play a very important role in BCC structures. In their study of the hydrogen desorption from ferrite and pearlite, Takai [47] found as hydrogen diffused inwards, it has to pass through layers of pearlite, which retards hydrogen permeation. This movement was also affected by weak trapping sites which include grain boundaries. Since diffusive hydrogen plays a deleterious role on steel microstructures, weak traps pose a problem as hydrogen can move through the lattice upon being freed from these types of traps. Moreover, the very small size of these grains means more intergranular surface is available thus leading to a larger amount of diffusion. Similar to 1018, 4340 possesses

microvoids of the same size within the microstructure. Once again, these voids are not a widespread feature and do not contribute greatly to the registered amount of hydrogen unlike the contributions from the grain boundaries and pearlitic regions of the microstructure.

Pure iron possesses a microstructure consisting of only ferrite grains due to the purity of the material. Figure 6 shows the pure iron microstructure at two different scales. The width of the grains range from 25-100 μm on average. Each grain possesses a different orientation with respect to adjacent grains. These much larger grains contribute to the ductility of the microstructure and significant reduction in hardness measurements as opposed to 1018 and 4340.

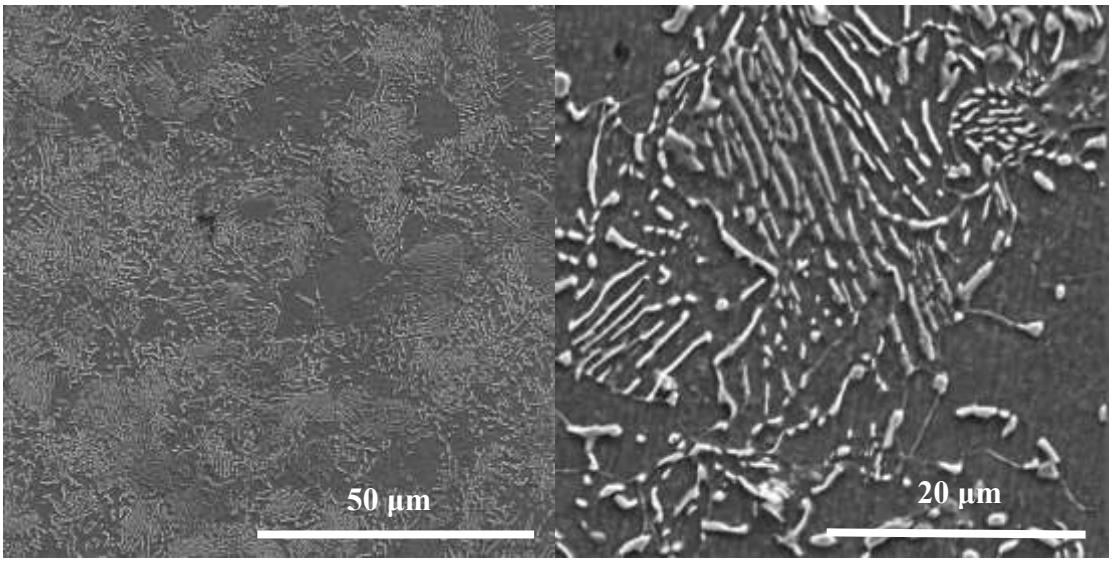

Figure 5: Secondary electron SEM images of 4340 microstructure. At 50 μm scale (left) and 20 μm scale (right).

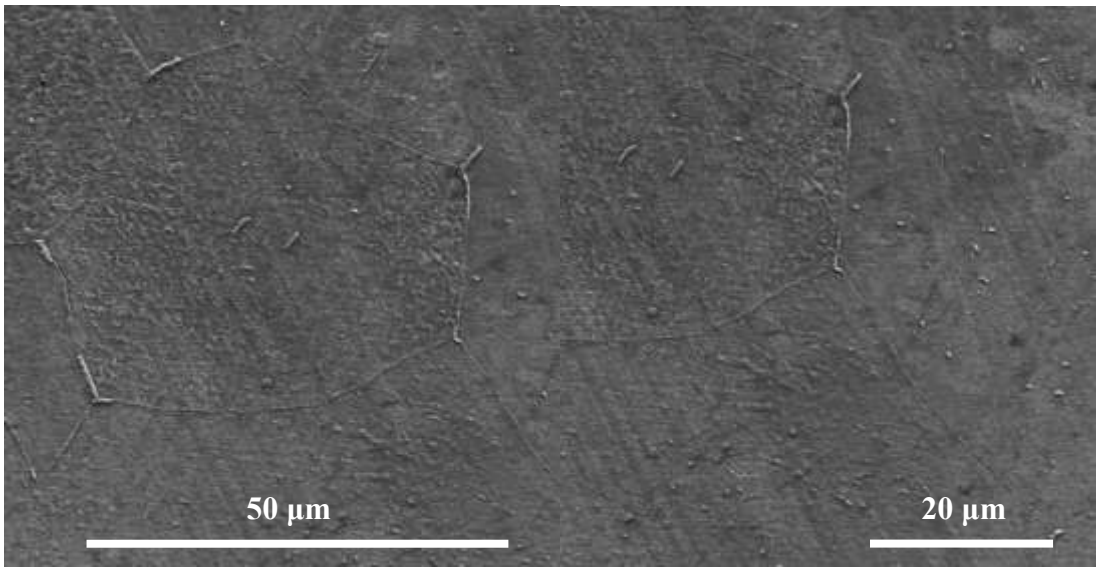

Figure 6: Secondary electron SEM images of pure iron microstructure. At 50 µm scale (left) and 20 µm scale (right).

IV.B Hydrogen Charge Analysis

Hydrogen charging of the steel and pure iron samples provided a look into the storage behavior of ferritic microstructures undergoing cathodic charging. Once charging was complete, the samples were burned in the Galileo. After the test time was complete, a hydrogen desorption profile was generated detailing the weight of the sample billet, the total hydrogen content, and the curve of desorption rate. Figure 7 and Figure 8 provide desorption profiles for 10 hours of charging for the two steels.

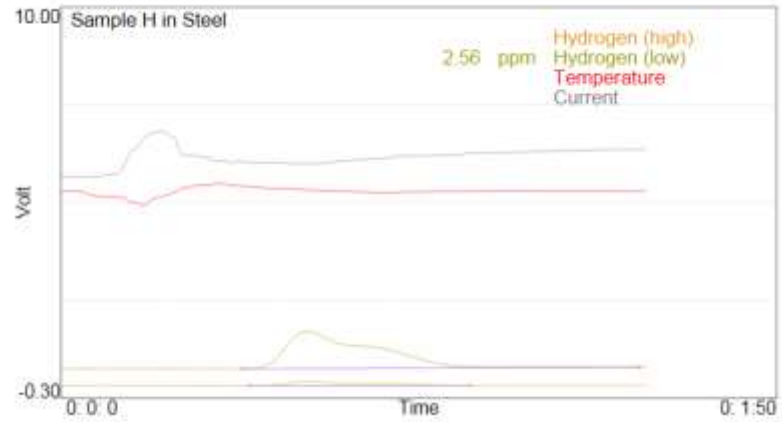

Sample code	: 1018 10 hr sample rd 3
Comment	: ---
Time	: 1:25:55 AM
Date	: 2/28/2017
Weight incl. unit	: 1.5160 g
Hydrogen (low)	
Result	: 2.55673 ppm
Factor	: 2514.0310
Blindvalue	: 0.0000
Blindvalue	:

Figure 7: Hydrogen content analysis for 10 hours of charging for 1018 steel.

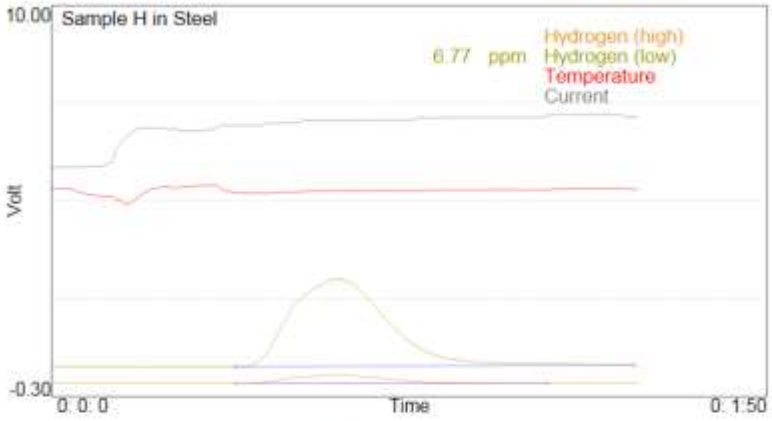

Sample code	: 4340 10 hr sample rd 3
Comment	: ---
Time	: 1:38:39 AM
Date	: 2/28/2017
Weight incl. unit	: 1.4958 g
Hydrogen (low)	
Result	: 6.76858 ppm
Factor	: 2514.0310
Blindvalue	: 0.0000
Blindvalue	:

Figure 8: Hydrogen content analysis for 10 hours of charging for 4340 steel.

Each analysis result generated by the Galileo provided the data for the diffusion profiles that were generated to determine permeability and trapping behavior of each microstructure. Over the range of charging times, 1018 and 4340 exhibited similar behavior up to 24 hours. Figure 9 and Figure 10 display the hydrogen storage behavior of 1018 and 4340, respectively. Initial charging times from 0-5 hours exhibit a steady increase in the amount of hydrogen. For charging times from 10-15 hours, the hydrogen content appears to saturate as the concentration of both 4340 and 1018 appear to stagnate. From 20-24 hours, 1018 and 4340 show a gradual increase in hydrogen content. However, after 24 hours, the hydrogen storage behavior of the two steels deviate. While 1018 appears to stagnate once again from the 24 hour to 30 hour mark, 4340 shows increasing values.

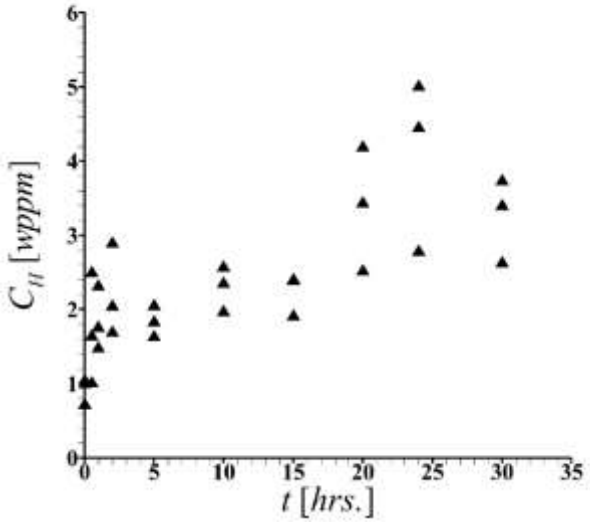

Figure 9: Hydrogen diffusion profile of 1018 steel.

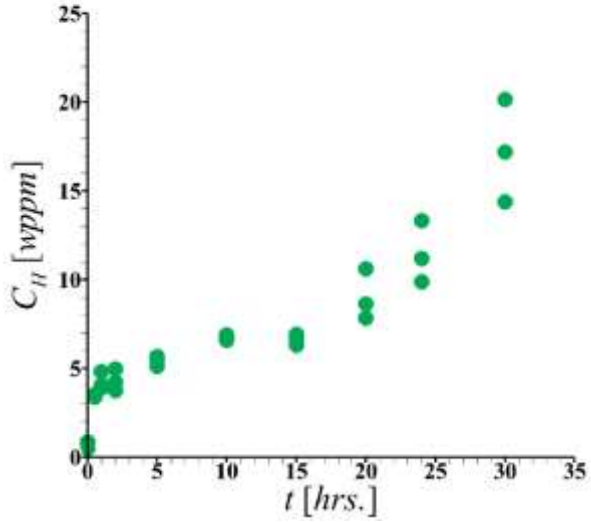

Figure 10: Hydrogen diffusion profile of 4340 steel

While the behavior may possess similar curves in terms of the hydrogen storage behavior analysis, the values in PPM for each steel varies greatly. During the initial charging periods of 0-5 hours, the amount of hydrogen in 4340 and 1018 does not deviate in the shape of the curve very much. Corrosion pits were observed to form at the bottom portion of the exposed area in 1018 and 4340 at the 2 hour mark as shown in Figure 11.

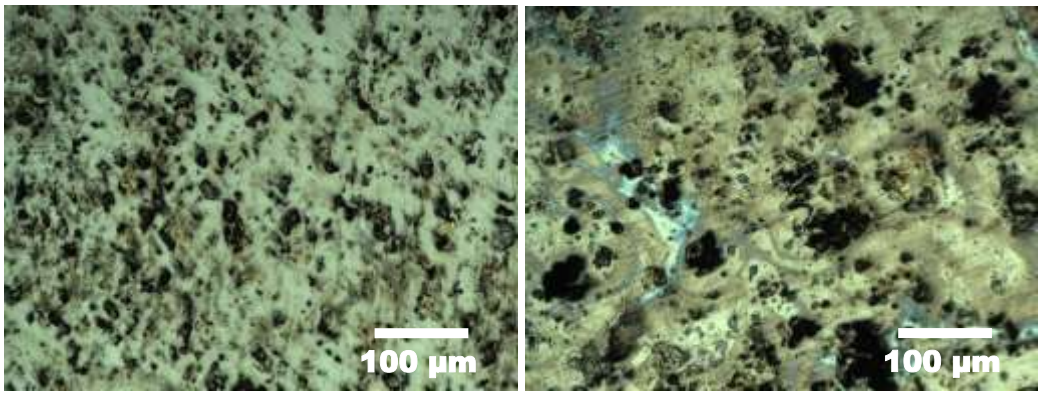

Figure 11: Corrosion pits in 1018 (left) and 4340 (right) after 2 hours of charging.

Upon increase to 10-15 hours, however, hydrogen diffuses through 4340 much quicker than in 1018. As mentioned before, this region of both curves exhibits a saturation in both materials. After the 15 hour mark, 4340 begins to gather much more hydrogen storing from 8-13 PPM as opposed to 1018 which remains within 2-4 PPM. 4340 begins to show the effects of corrosion at 30 hours of charging as some samples were charged to the point that the structure eroded into smaller sample pieces at the end of charging. Most notably, the more intact samples exhibited a large corrosion crater where a sizable amount of sample was missing. A pit formed at the exposed bottom flat surface of the sample. While no analysis was made to determine the amount of deterioration as a function of hydrogen content, it may prove pragmatic to undertake such a study in material degradation in order to further assess the macroscopic catastrophic failure that may occur. On the other hand, 1018 did not exhibit macroscopic degradation other than corrosion pits that formed at the bottom face of the exposed area. These samples also remained intact throughout all of the periods of charging.

The difference in the amount of hydrogen content in each steel can be attributed to the variance in the microstructures of each steel. As 4340 steels feature a larger amount of grain boundaries in the microstructure, these inhomogeneities act as trapping sites for hydrogen. Some defects present in the lattice other than grain boundaries also contribute to the larger amount of hydrogen present in the lattice. Furthermore, the two forms of pearlite in the microstructure most likely aid in the trapping of hydrogen observed in the initial charging periods. These sites saturate quickly leading to the first observed saturation limit at the times before 15 hours. At ambient temperature, the main path for hydrogen diffusion in a ferrite-pearlite structure is along ferrite grains or interfaces between ferrite and pearlite. Pearlite colonies in ferrite act as effective barriers to hydrogen diffusivity [48]. Pearlite blocks that exist at ferrite layers are possible obstructions to hydrogen diffusion in the banded ferrite-pearlite structure. Hydrogen primarily travels through the ferrite layer and along ferrite grain boundaries and ferrite-pearlite interfaces [48] [49]. This would explain the consistently larger hydrogen content measurements characteristic

of 4340 throughout the periods of testing. At longer charging times, the dislocations present in both materials begin taking on hydrogen. These sites typically exhibit smaller binding energies which contributes to their lack of activity during saturation of the pearlitic cementite. The macroscopic degradation of 4340 results from continued charging may be due to internal damage caused by the charging current. In theory, 4340 may be more susceptible to the influence of electrolytic environments leading to galvanic corrosion. This type of corrosion is the result of two electrochemically different metals in close proximity that are submerged in an electrolyte [50]. This conclusion is reasonable since the samples were the anode during the charging experiments. Anodes corrode at a faster rate than cathodes which may not corrode at all. The platinum counter electrode did not experience any corrosion, however, the carbon based electrodes used to the test the validity of the electrodes did corrode at longer charging times. This is due to the movement of metal ions through the electrolyte from anode to cathode. As a corollary, the coagulation of corrosion product can impede the movement of hydrogen in steels which also may have resulted in the much higher hydrogen content results.

1018 steels feature a microstructure that is ferritic dominant as opposed to that of 4340 which contains ferritic regions surrounded by large agglomerations of pearlite. 1018 does possess some pearlitic regions as well which most likely trap hydrogen. Since the microstructure is primarily ferritic, most of the hydrogen gathers at dislocations and grain boundaries similar to the behavior of pure iron. This implies that hydrogen is diffusing through the lattice. Hydrogen diffusivity in ferrite-pearlite structures is ascribed to carbide distribution consisting of cementite lamellae in the pearlite which diminishes the movement of hydrogen through the microstructure [51]. Since the microstructure is more ferrite than pearlite, hydrogen is most likely becoming trapped at these pearlite colonies as observed in [48]. This would lead to the conclusion that 1018 does experience hydrogen embrittlement. Hydrogen coagulates in surface regions which causes the pitting that is observed during the longer charging times. However, the microstructure does promote the transportation of hydrogen deeper into the specimens which would explain the charging values remaining within a similar range to pure iron.

Diffusivity of H in pure and non-deformed α-iron at room temperature is very high above $1x10^{-4}$ cm^2/sec [6]. The diffusion of hydrogen into the pure iron lattice shows a quick diffusion into the microstructure. However, the PPM value appears to level off immediately (within 0.5-1 hour) showing that hydrogen diffuses quickly but the value remains stagnant despite increasing charging time. Figure 12 provides the hydrogen diffusion behavior in pure iron. There is a small increase as the charging time approaches 2 hours. Accompanying tests were performed at 3 hours to confirm saturation behavior of the hydrogen in the pure iron lattice. As expected, charging pure iron for 3 hours did not increase the amount of hydrogen present in the lattice. Further tests were conducted at longer times of 5, 10, 15, 20, and 24 hours to determine the validity of the previous analysis. In accordance with the previous findings, longer charging times did not further saturate the lattice with hydrogen, rather the PPM content of hydrogen within the lattice remained within the same range as those times when hydrogen content initially saturated.

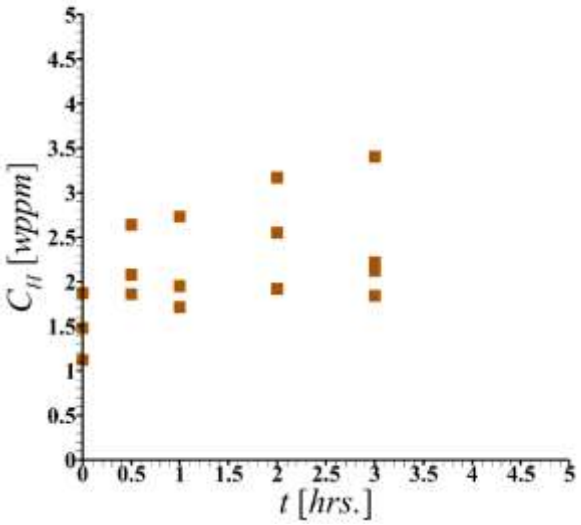

Figure 12: Hydrogen diffusion behavior of pure iron

This saturation behavior can be understood better upon considering the microstructure of pure iron. Like both of the previous materials considered, pure iron contains some amount of dislocations that contribute to the trapping behavior observed. Dislocation cores in pure iron are more likely to become prevalent hydrogen containers as these structures do not feature the lamellae regions that 1018 or 4340 do. Since pure iron features large grains that possess a high degree of homogeneity due to the purity of the material, some of the hydrogen that penetrates the lattice coagulates at the grain boundaries accounting for some of the hydrogen concentration reading in the pure iron lattice determined by the G8 Galileo. Hydrogen is reported to move through the ferritic lattice as proton to move through the interstitial sites. These interstitial sites most likely saturate quickly according to the hydrogen storage profile above. Moreover, high concentrations of hydrogen form at the core of edge dislocations in BCC metals.

Since the hydrogen content measured during analysis saturates despite increased charging times, it is suggested that hydrogen does not get trapped within the pure iron samples studied here. Pure iron is proposed to be susceptible to hydrogen embrittlement due to the high hydrogen diffusion coefficient in ferrite. Though diffusible hydrogen content is low for pure iron, hydrogen atoms can move great distances through the lattice which subsequently aids the degradation of mechanical behavior due to hydrogen [13]. Since ferrite comprised 99.7% of the composition, it can be inferred that the low hydrogen content measured here correlates with a large amount of hydrogen diffusing through the lattice. This effect occurs quickly as hydrogen content saturated within 1-2 hours of charging. Thus, the exposure of pure iron or other primarily ferritic microstructures may encounter similar hydrogen diffusion issues. As is referenced in various works, the movement of hydrogen through the lattice is a precursor to hydrogen embrittlement.

V. NANOINDENTATION

Surface analysis of the three specimens was performed through nanoindentation methods. Samples were indented using the TI 950 Triboindenter. This nanoindentation device provided a high load transducer apt to penetrate the steel specimens before and after charging was performed. The low load transducer was unable to provide accurate readings due to a lack of penetration depth exhibited by the probe. Nanoindentation helped determine the hardness and reduced elastic modulus of the sample as determined through fitted curves generated by the Triboscan software. The Triboindenter indents on a polished portion of the sample using a Berkowicz triangular tip. The high load transducer must also be calibrated with a test sample before indents can be made in order to ensure that the area function chosen produces proper results. The test sample chosen for the high load experiments was fused quartz. The area functions utilized by the software were calibrated before each test to ensure accuracy of results.

To understand the effect of hydrogen on mechanical properties of the three ferritic structures, a time span was chosen for each type of material depending on the results obtained by the Galileo. For the steel samples, charging times of 1, 2, 5, 10, 15 and 24 hours were chosen to capitulate the influence that hydrogen possesses on hardness and reduced modulus with respect to the storage behaviors observed in the previous section. Pure iron similarly was charged for 1 and 2 hour time periods but also was subjected to a three hour period to corroborate the accuracy of saturation results as observed by the Galileo.

For the control sample, indentation occurred after a typical grinding and polishing procedure similar to that performed during metallographic characterization. Steel samples were first ground with 360 and 500 grit papers to remove residual products from sample fabrication. Due to the more pliant nature of pure iron, these samples underwent the same grinding procedures but with much less force to ensure no work hardening results would be read by the nanoindenter. As nanoindentation requires a properly polished surface, all three samples were subjected to polishing procedures starting from 9 to 6 to 1 μm polishing cloths to be certain of an adequately prepared surface. Once the polishing procedures were

completed, samples were taken to the Triboindenter. Charged samples required a different procedure due to the proclivity of the samples to develop corrosion pits even at relatively short durations.

In order to capture the complete array of mechanical properties of the specimens, considerations were made to ensure that indents fell on differently oriented grains or other material phases. This indent pattern ensured that a more precise measurement of the effect of hydrogen on hardness and reduced modulus of specific phases in the material. It has been proposed that a synergistic effect of adjacent phases can create a considerable difference in mechanical properties. Thus, choosing a proper value for spacing between indents was not only pragmatic but an integral part to offering a comprehensive effect of deformation behavior after hydrogenation.

Indents were made through a 25x25 grid at varying distances depending on type of sample. The steel samples featured regions of smaller grain sizes interspersed with regions of medium grain sizes. This required a much smaller between indent spacing of 50 µm. For pure iron samples, which possessed much larger grains, a between indent spacing of 75 µm was chosen as this fell within a larger portion of the range of grain sizes. Figures 13 present images of the nanoindentation paths for both types of specimens used in the study.

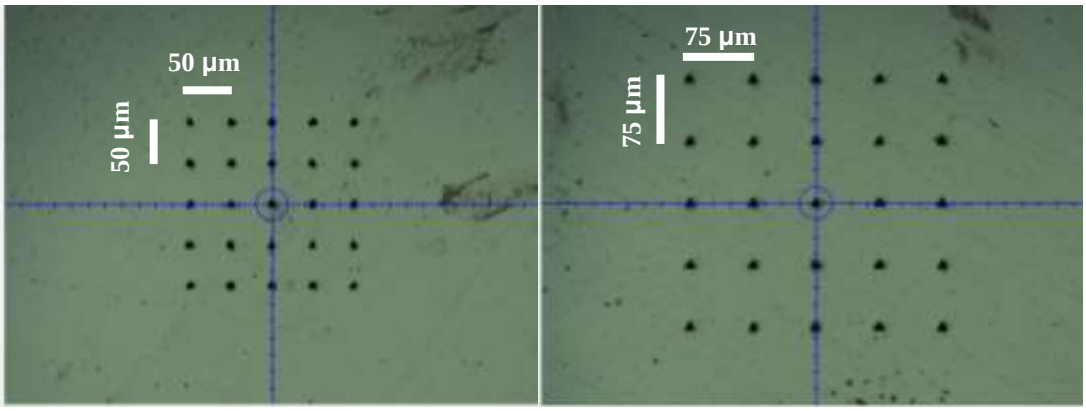

Figure 13: Nanoindentation paths for both types of materials used in study. Path for steels (left) used grids of 25x25 with 50 µm spacing. Path for pure iron (right) used grids of 25x25 with 75 µm spacing.

Indentation results from the Triboindenter indicate that charged samples were prone to increases in hardness associated with hydrogen embrittlement. The pure iron sample appears to be the least susceptible to hardness increase, while displaying similar saturation behavior in hardness increase to that of its hydrogen absorption curve. 4340 exhibits an increase in hardness upon first charging up until 10 hours. After 10 hours, a sharp decline occurs at 15 hours. At 24 hours, a large amount of softening is observed that drops the hardness below the original uncharged sample value. As the charging profile of 4340 shows, a saturation occurs during the 10 to 15 hour charging times. This may be due to certain trapping sites that are not immediately saturated upon the inception of hydrogen to the system being filled by travelling hydrogen as it moves into the bulk. Upon longer charging times, hydrogen can infiltrate the crystal structure further moving past the now saturated sites remaining below the surface. After the 15 hour mark, free roaming hydrogen from the electrolyte cannot locate to these now filled energy wells and tunnels further into the bulk to repeat the process. Since the nanoindentation was performed on the exposed surface to the electrolyte, the results of 4340 may denote that hydrogen may have penetrated into the bulk of the sample by the 10 hour mark and subsequently reducing the hardness as charging time increases. 1018 experiences an increase at the 1 hour mark and experiences slight increases until the 10 hour mark. After the ten hour mark, the hardness of 1018 begins declining as the charging time increases. This may indicate a softening mechanism begins to occur after 10 hours. When compared to the results of charging, it can be seen that the slight decrease coincides with a slight increase in hydrogen content of 1018. While the hardness does not fall below the threshold of the non-charged sample, the decline is similar to the behavior of 4340 although not as pronounced.

To determine whether this softening was due to hydrogen specifically, the 24 hour samples were baked at 175 C for 24 hours to remove hydrogen from the lattice. Next, the samples were indented once more at a location far from the initial group of indents. These tests yielded interesting results as the hardness of 1018 jumped back up to the value at the 10 hour mark while the hardness of 4340 actually decreased slightly.

The observed behavior of 1018 and 4340 after 10 hours may be due to the HELP mechanism which dictates lower mutually repulsive interactions cause material softening. Sofronis describes the HELP mechanism to be a process that produces a highly localized plastic failure rather than embrittlement. In this case, macroscopic ductility is limited by the beginning of an extensive localized plasticity [52]. While the work performed did not measure macroscopic mechanical properties, the nature of nanoindentation lends to the proposition that the local deformation of the hydrogen imbued sample led to an observed softening in the surface region exposed to the electrolytic solution. Perhaps, the non-reversible deep traps are saturated quickly at the surface of the material and bulk before another type of trap becomes the dominant mechanism that draws in hydrogen. From their review, Sofronis reports that upon deformation grain boundaries with the highest concentration of hydrogen exhibit regions that deform at the lowest stresses leading to plasticity occurring in the vicinity of boundaries rather than at the boundaries themselves. Thus, as 4340 absorbs the largest amount of hydrogen, it can be proposed that the pearlitic cementite lamellae and dislocations are trapping hydrogen at the surface level and past a certain depth in the bulk leading to a pronounced softening that occurs as charging time increases. These sites are then most likely not the first sites to be filled with hydrogen. It is also possible that the large decline experienced by 4340 specifically was spurred by internal corrosion gas bubbles that may have weakened the infrastructure of the sample below the surface. Since the bottom portion of the sample experienced grinding by a high grit sand paper, this region promoted adsorption to the sample surface more so than at the circumferential area of the sample sides. This would run parallel to the macroscopic degradation of the 4340 samples seen after 30 hours of charging. Another explanation is that certain microstructural phases are more effected by the presence of hydrogen. Thus, as the indentation was performed, a larger portion of these susceptible grains were indented resulting in a drop off in strength. Furthermore, since individual grains may be randomly oriented with different planes residing adjacent to each other, the indentation results may be affected by orientation effect of neighboring phases. This proposal incorporates the presence of individual phases' susceptibility to hydrogen as well as the

HELP mechanism. Analysis of the differences between the two steels would point to the differences in the microstructural phases as well as the amount of phases and grain boundaries to be determining factors to the susceptibility of steel to hydrogen. This would further explain the precipitous hardness decrease displayed by 4340 upon longer charging times. Figures 14 – 16 display the results obtained from the mean hardness and standard deviation calculation provided by the multiple curve analysis data generated by the Triboindenter.

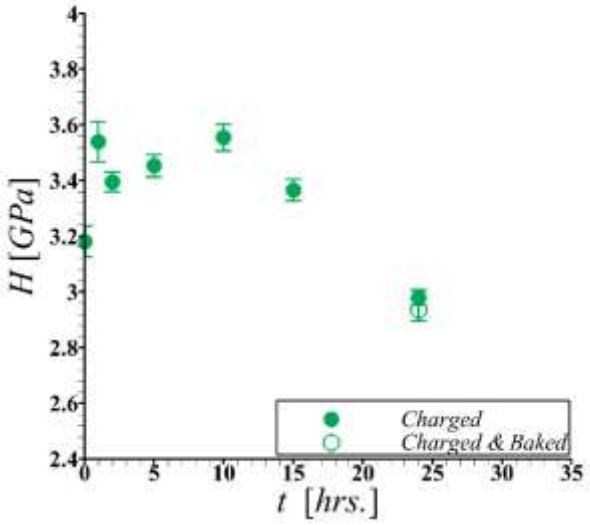

Figure 14: 4340 hardness vs charging time

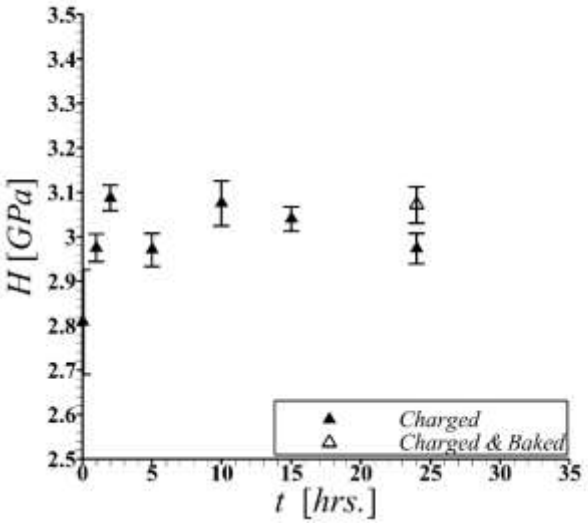

Figure 15: 1018 hardness vs charging time

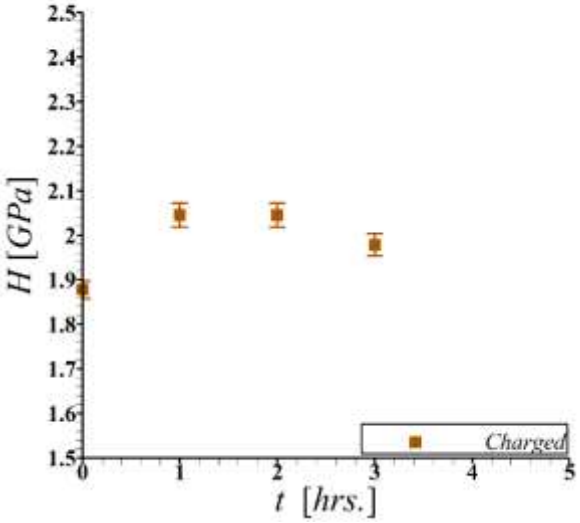

Figure 16: Pure iron hardness vs charging time

The Triboindenter also provided a measure of the reduced modulus which was then compared to time of charging to additionally quantify the influence of hydrogen. Hydrogen was not expected to have an influence on the reduced elastic modulus value, however, a correlation to the results in the hardness measurements was sought to further elucidate the effects of hydrogen on mechanical properties. Pure iron appeared to experience a drop in reduced modulus that remained consistent between the three charging times. 4340 and 1018 appear to experience opposite effects to the reduced modulus as a result of hydrogenation. The reduced modulus of 4340 appears decrease to a range of saturation. 1018 experiences an increase in reduced modulus and remains within a range of saturation henceforth. Figures 17 – 19 provide the reduced modulus versus charging time data obtained during the nanoindentation of the three types of specimens at the four different charging times. To better capitulate the effect of hydrogen on the mechanical properties of each material without orientation of crystallographic planes affecting measurements, the proportion between hardness and the reduced modulus squared is plotted against time. This was performed in order to homogenize the effect of grain orientation on the measurements of hardness and reduced modulus. Figures 20-22 present the plots for each specimen. Each plot is plotted with error bars to show precision in measurements by the Triboindenter. Similar to the previous results of 1018 and 4340, neither material showed a systematic trend for this H/E^2 value. Pure iron, on the other hand, did display an immediate increase before tending to saturate as charging time increased. The effects of hydrogen on the mechanical properties of steels specifically those measured through nanoindentation are a subject worth further study after the work performed here as a consistent behavior could not be assessed.

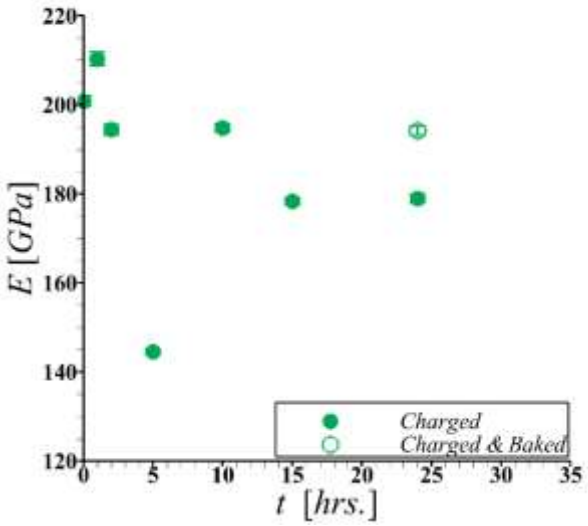

Figure 17: 4340 reduced modulus vs charging time

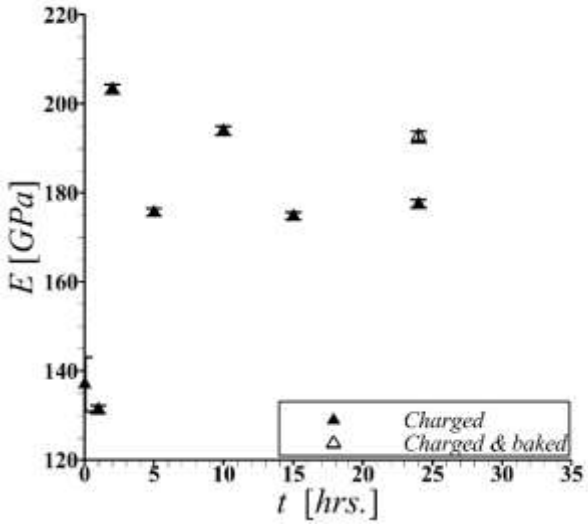

Figure 18: 1018 reduced modulus vs charging time

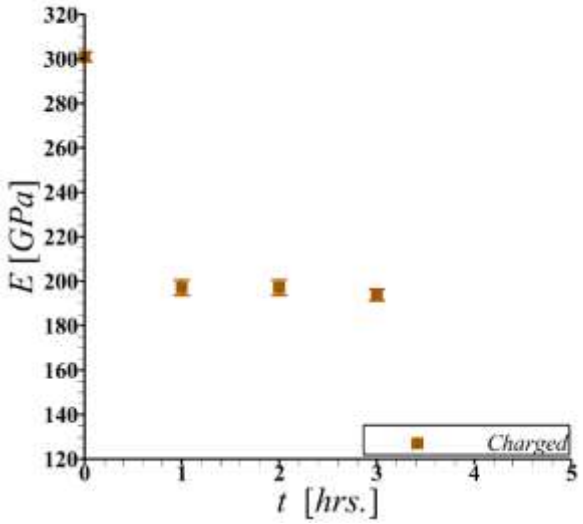

Figure 19: Pure iron reduced modulus vs charging time

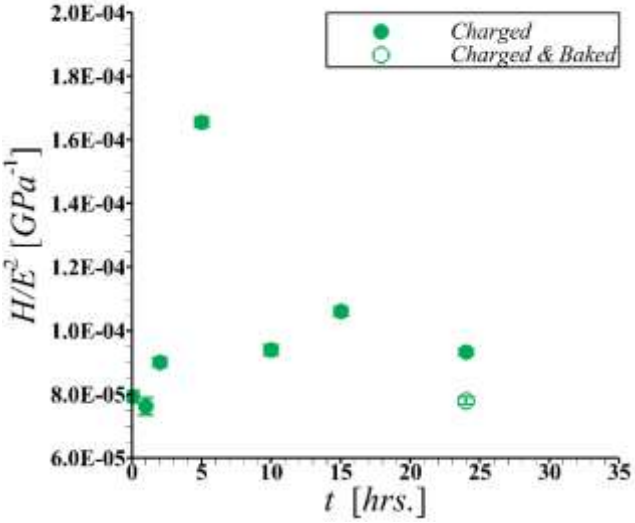

Figure 20: 4340 hardness over reduced modulus squared vs charging time

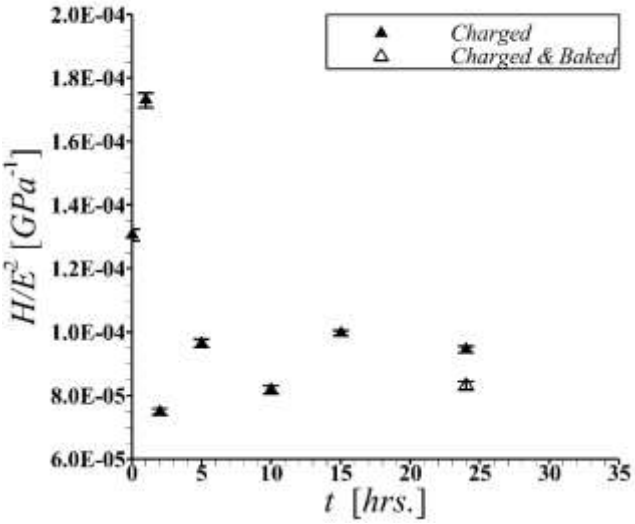

Figure 21: 1018 hardness over reduced modulus squared vs charging time

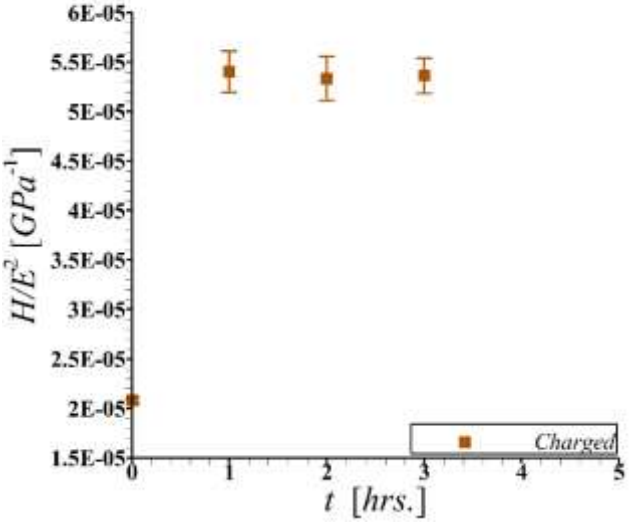

Figure 22: Pure iron hardness over reduced modulus squared vs charging time

VI. MODELING OF HYDROGEN THERMODYNAMIC DIFFUSION

VI.A Background and Previous Work

An accurate description of the diffusive behavior of hydrogen in the three different microstructures was desired to help make predictions of the susceptibility of each ferrite based structure to hydrogen. Despite a wealth of experimental data, a model that accurately determine how hydrogen traps in a steel microstructure and which features are predominant in the mechanism of storage. Hydrogen transport can be distinguished between three key phases: penetration, storage, and release. As hydrogen interacts with a steel, it first encounters an energy well that acts as diffusion sites for further ingress in the metal at the surface of the material. The diatomic hydrogen breaks down into a singular atomic form that can easily move through the lattice. Traps represent another binding site that hydrogen must escape to diffuse farther. These sites possess energies larger than that required for lattice diffusion.

Modern hydrogen diffusion models have shown that Fick's laws of diffusion can be integrated with considerations to the effect of microstructure and charging conditions on the concentration of hydrogen and diffusion coefficients. The influx of hydrogen through a structure can be first modeled using Fick's first law of diffusion:

$$J_x = -D\frac{dC}{dx_x}$$

The mechanism of hydrogen storage typically observes hydrogen atoms occupying interstitial lattice sites and microstructural trap sites associated with microstructural features including dislocations, grain boundaries, and inclusions. The probability that a trap is occupied depends on its binding energy and hydrogen concentration at surrounding lattice sites. When traps have large binding energies, hydrogen is more likely to be captured and less likely to be released. Sofronis and McMeeking [53] found that hydrogen populates at normal interstitial lattice sites (NILS) or at reversible sites that are created by plastic deformation. Oriani [10] postulated that the two sites possess a hydrogen concentration equilibrium. Oriani's theory comes with the assumption that no interaction occurs between occupied sites and that local equilibrium exists between hydrogen

concentration in the lattice and at traps. This model has been shown to have shortcomings in determining the entire phenomena measured during proceeding experimental procedures [54] [55] [56]. However, from this assumption, a relation was developed by Galindo-Nava et al. between equilibrium concentration in the lattice (c_L) and traps (c_t) as well as an effective diffusion coefficient estimation that considers the effect of traps [57]:

$$c_t = c_L \frac{N_t}{N_l} \exp\left(\frac{E_b}{R_{gas}T}\right)$$

$$D = \frac{D_0 \exp\left(-\frac{Q}{R_{gas}T}\right)}{1 + \frac{N_t}{N_l} \exp\left(\frac{E_b}{R_{gas}T}\right)}$$

N_l and N_t represent the total lattice and trapping sites in the material, respectively, E_b is the trap binding energy with hydrogen, D_0 is the lattice diffusion coefficient prefactor, Q is the activation energy for hydrogen lattice diffusion, R_{gas} is the gas constant and T is the temperature.

As various models exist, the scatter in reported trapping parameter values makes predicting susceptibility of hydrogen embrittlement due to the existence of multiple trap types affecting the diffusivity of hydrogen a difficult task. This task is complicated further upon consideration of electrochemical permeation charging conditions that may affect the apparent diffusivity of hydrogen in the material. Despite the lack of a unified theory, it can be agreed that local equilibrium may exist for a period of time and length scales for electrochemical charging and thermal desorption processes. Furthermore, the diffusion models proposed by Fick are able to quantify hydrogen diffusion.

In the work of Galindo-Nava et al., a unified hydrogen transport model that incorporates electrochemical permeation, thermal desorption and degassing is proposed [57]. The work performed herein focuses on the permeation model for ferritic structures. This model utilizes Fick's diffusion equations while considering microstructural features, electrochemical charging and test parameters, and three-dimensional geometries that determine the overall diffusion behavior. By using the local equilibrium assumption by

Oriani, a diffusion coefficient is estimated with respect to hydrogen outgas with microstructural sites acting as hydrogen traps. Alloy grades of similar microstructures are modeled by fitting them with the same sets of parameters. The model proposed is complementary to the work performed here as the modelling considers electrochemical charging for measurement of hydrogen permeation rate and apparent diffusion within a metal.

Two regimes are generated during hydrogen ingress. The first is the transient region induced by electrochemical reactions at the sample's surface. The second is a steady state where the variation in concentration and current density is constant. Electrochemical charging is known to increase hydrogen content in a structure to help understand trapping behavior. Fick's diffusion equations are able to be used if the oxide layer that is generated during charging is considered as an additional energy barrier to diffusion [58] [59]. This assumption is valid for sample thicknesses that exceed ~0.1 mm. [59] [60] As the cylindrical billets used here exceed that value, the mechanism proposed is valid for modeling hydrogen diffusion in the ferritic structures studied here.

Hydrogen diffusion profiles are generated by considering the density of traps and activation energy for oxide formation which affords movement through the lattice. After entering the sample, individual hydrogen atoms diffuse through the lattice until they reach a trap (concentration well). The trap landscape depends on microstructure which is described by the function $c_{well}(x)$. The saturation concentration is $c(x) = c_{sat}$ for x within trapping wells. For x different from x_0, $c_{well}(x) = 0$. Hydrogen first sticks to traps until the site saturates. Any hydrogen leftover diffuses across the lattice until depositing at the next trap. Another energy barrier that occurs at traps may also need to be overcome [61], but is considered negligible due to the limited amount of information on its effects on the diffusion profile. The typical inhomogeneity of the energy landscape that affects hydrogen diffusivity is not quantified in this work to help define an effective diffusion coefficient. Thus, a homogeneous trapping landscape is considered that can help calculate D in the permeation diffusion equation due to the assumption of local equilibrium between free and trapped hydrogen atoms.

For electrochemical permeation, a mass flux J can be calculated by determining the difference between mass flux going to the wells J_{well} and mass flux that occurs by electrochemical charging J_{perm}. The equation is provided below:

$$J = -(J_{well} - J_{perm}) = -D_{perm}(\nabla c_{well} - \nabla c_{perm})$$

D_{perm} is the apparent diffusivity during permeation. ∇ is the three dimensional differential operator. Through Fick's second law of diffusion, hydrogen permeation rate can be obtained:

$$\frac{dc_{perm}}{dt} = D_{perm}(\nabla^2 c_{well} - \nabla^2 c_{perm})$$

For the cylindrical samples studied in this work with radius R and length L, which can be expressed as a set of three ordinary differential equations that depend on time t, R, and Z which can be solved through typical methods. This equation is provided below:

$$R_n Z_m \theta'_{mn} = D_{perm}(c_{sat} - \theta_{mn})(R''_n Z_m + \frac{1}{r} R'_n Z_m + Z''_m)$$

If no hydrogen exists within the sample, the initial parameters are set $c_{perm}(r, z, 0) = 0$. The boundary conditions used by Galindo-Nava represent constant concentration at the surface of the sample since distribution of traps establishes steady state permeation flux. When $c_{perm}(R,z,t)=c_{sat}$, the $dc_{perm}/dr(R, z, t) = 0$ and $c_{perm}(r, -L/2, t) = c_{perm}(r, L/2, t) = c_{sat}$, $dc_{perm}/dz(R, -L/2, t) = dc_{perm}/dz(R, L/2, t) = 0$. The solution for this equation with these conditions is given by infinite series:

$$c_{perm}(r, z, t) = c_{sat} \sum_{m,n=0}^{\infty} (1 - \exp(-D_{perm}(\lambda_n^2 + \alpha_m^2)t))R_n Z_m$$

While various works have mentioned the effect of microstructure on the diffusivity during permeation, this value is also correlated to the square root of the charging current density Ic [62] [63]. D_{perm} is also known to increase when trap density increases [54] [55] or when traps have high binding energies [56]. The equation of the effective diffusion coefficient has the form:

$$D_{perm} = D_{perm,0}\sqrt{I_c}(1+\frac{N_t}{N_l}\exp(\frac{E_b}{R_{gas}T}))\exp(-\frac{E_{perm}+Q}{R_{gas}T})$$

$D_{perm,0}$ is the effective diffusion coefficient prefactor. E_{perm} represents the increase in the energy barrier due to hydrogen permeation. When adjusted for ferritic, martensitic, bainitic and pearlitic steels, $D_{perm,0}$ = 1.16 x 10^-11 m^3/A-1/2 s-1. Hydrogen saturation concentration c_{sat} increases with the steady state permeation density I∞ through the increase in charging density (I_c) from the experiments performed by [28] [58] [64] [65] [66]. For the purposes of this study, saturation concentration in trapping wells is determined by approximation from the experimental results provided by the Galileo.

VI.B Correlating Trapping Phenomena with Microstructure

A variety of works have estimated the binding energy of different microstructural features through experimental and simulated means. Unfortunately, the distribution range in energies is large. For specific microstructural features, a number of interesting parameters exist with respect to observed experimental results. Pearlitic structures, which feature lamellar cementite, have a higher binding energy due to its inclination to alter the patterns of hydrogen movement [67]. While the interfaces between ferrite and cementite does possess considerable trapping potential, hydrogen is more likely to become trapped at the lamellae interiors. The frequency at which hydrogen in the lattice encounters trapping sites is noted to be proportional to the mean spacing Λ between respective microstructural features. Dislocations possess a Λ that adheres to the mean dislocation spacing ($1/\sqrt{\rho}$) where ρ is the dislocation density and the width of trap r_t is given by r_t = πb [68] where b is the burgers vector. Grain boundaries have Λ that equals the mean grain size D_g and r_t = b [68]. Finely dispersed spherical precipitates requires a different derivation, $\Lambda_p = r_p\ (\frac{\pi}{f_p})^{(\frac{1}{2})}$ where r_p is the mean radius and f_p is the volume fraction. As hydrogen can be trapped at any part of the precipitate's interface, another factor equaling

the surface area width per unit volume is included $\frac{A_p b}{V_p} = \frac{3b}{r_p}$. r_t equals half of the arc length of the particle πr_p. The number density of these traps are provided below:

$$\frac{N_{dis}}{N_l} = \frac{\pi b}{\Lambda_{dis}} = \pi b\sqrt{\rho}$$

$$\frac{N_{grain}}{N_l} = \frac{b}{\Lambda_{grain}} = \frac{b}{D_g}$$

$$\frac{N_p}{N_l} = \frac{\pi r_p}{\Lambda_p}\frac{A_p b}{V_p} = \frac{3\pi^{1/2} f_p^{1/2}}{r_p}$$

The total concentration of hydrogen can be estimated through addition of the individual desorption peaks in TDS of non-interacting traps that exist in the specimen [56] [69]. Modeling results by Fischer et al. corroborates that the hydrogen content is the sum total of trapping contributions existing in the sample [70]. The linear nature of Fick's diffusion equations allows the hydrogen concentration when multiple traps exist equals the sum of the contribution from each individual type of trap. A trapping well that has different kinds of traps is the sum of the wells where each kind of trap has a saturation concentration. The permeation concentration is split into the permeation concentration that comes from each trapping well. Thus, the concentration evolution that exists during the three processes of hydrogen movement through the microstructure with respect to different types of traps is provided here:

$$c_{perm} = \sum_i c_{perm,i}$$

$$c_{perm} = \sum_i c_{\deg as,i}$$

$$\frac{dc_{desorp}}{dt} = \sum_i \frac{dc_{\text{de}\,sorp,i}}{dt}$$

From the data received by the Galileo, the model is able to quantify the hydrogen storage behavior that was observed during the various charging times. As was mentioned previously, the data shows an initial saturation that occurs within 0.5-1 hours before a

second period of increase in both steel structures at about the 15 hour mark. This would coincide with the model that predicted that pearlitic cementite lamellae would be saturated first before dislocations would begin to saturate. Figures 23 and 24 present the model prediction compared against the experimental results of the charging profile for 1018 and 4340, respectively.

Pure iron also exhibits a quick saturation for the time period observed. Figure 25 presents an image of the model with parameters fit to the experimental data of pure iron. This data was simply modeled as the trapping behavior of the dislocations in pure iron as prescribed in the original model. This may imply that pure iron exhibits a higher binding energy than was utilized in Galindo-Nava et al.

With the addition of this model, the phenomena of hydrogen permeation can be more accurately quantified. As predicted, the higher binding energy traps are more likely to saturate first. Since these sites typically feature lower saturation concentrations, they are filled quickly before hydrogen saturated dislocations can contribute to the overall hydrogen content. This would also coincide with the data from the nanoindentation results if the HELP mechanism is considered to be a prevalent factor at the 15 hour mark, when dislocations are predicted to begin taking on hydrogen. Thus, the Galindo-Nava model provides a succinct description and prediction of microstructural effects in steels.

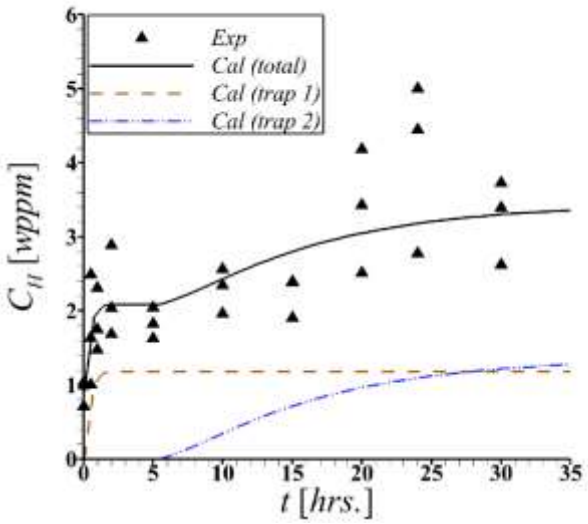

Figure 23: Model prediction of hydrogen charging of 1018 vs experimental results.

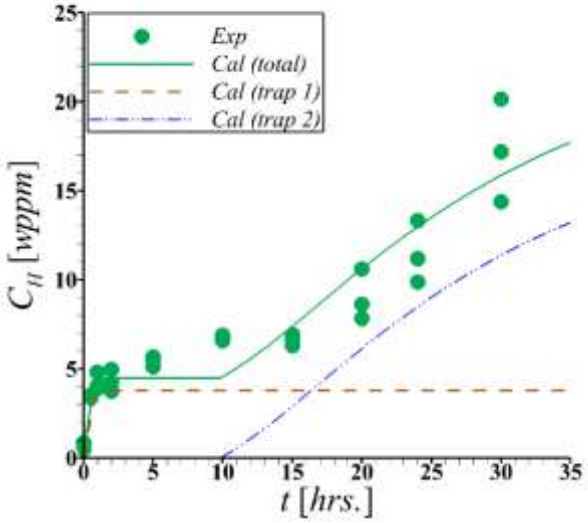

Figure 24: Model prediction of hydrogen charging of 4340 vs experimental results.

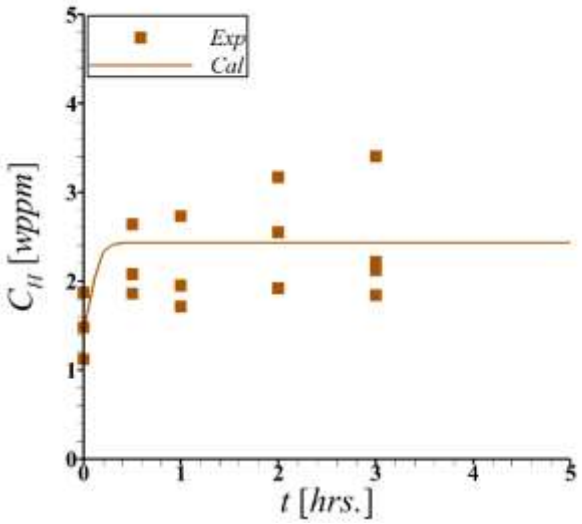

Figure 25: Model prediction of hydrogen charging of pure iron vs experimental results.

VII. CONCLUSION

In the work performed here, a study of the hydrogen permeation behavior and subsequent embrittlement characteristics was undertaken to develop a more adequate understanding of the mechanisms governing the effects of hydrogen on a steel lattice. A comprehensive analyses of the effect of microstructural features on hydrogen absorption in steels have been carried out. Hydrogen was introduced into the billets of two steels and pure iron through electrochemical charging. The total hydrogen content of each charged billets was then quantified following a gas fusion analysis principle known as melt extraction. The mechanical properties of the hydrogen charged billets of the three materials were characterized using nanoindentation technique. Thermo-kinetic modeling of hydrogen absorption in these materials was also carried out.

The observations from this work indicate that total absorbed hydrogen content in pure iron initially increases with charging time and then tends to saturate. On the other hand in 1018 and 4340 steels, following initial saturation, hydrogen content tends to increase again with continued charging. For a given charging condition, the total absorbed hydrogen in pure iron is always less than 1018 steel which is less than 4340 steel. The nanoindentation hardness normalized with reduced modulus squared (H/E^2) value for pure iron initially increases with charging time and then tends to saturate. On the other hand, in 1018 and 4340 steels the H/E^2 values do not show any systematic trend.

The thermo-kinetic modeling of hydrogen absorption in these materials further in understanding the correlation between hydrogen absorption and microstructural trapping sites present in these materials. The modeling results show that compared to pure iron, in 1018 and 4340 steels, there are potentially more than one trapping site. The additional trapping sites, which is conjectured to be pearlite, lead to an increased hydrogen absorption capability in 1018 and 4340 steels compared to pure iron. In 4340 steel, the second trapping site starts to absorb hydrogen after 10 hours compared to 5 hours in 1018 steel. The presence of a high volume fraction of pearlite in 4340 steel compared to 1018 steel results in high hydrogen absorption capacity.

This is consistent with the amount of heterogeneity of the steel microstructure as these regions of interwoven cementite lamellae act as hydrogen accumulation sites. Furthermore, the pearlitic regions act as sites from which hydrogen can gather causing further degradation. The amount of pearlite and phases prevalent in 4340 as well as other heterogeneities are the major contributors to the difference in hydrogen permeation susceptibility between 4340 and 1018. This can be further confirmed by the hydrogen storage behavior of pure iron which contains only ferrite grains and saturates rather quickly. Since 4340 features a larger portion of sites that can act as hydrogen reception regions, the amount of measured hydrogen is larger as time of charging is increased up until the point of the degradation of the steel.

As an extension of future work, a further investigation into properly determining the influence of hydrogen on steel microstructure should be undertaken. In this revised study, the steels would be charged and nano-indented in-situ. This work could be performed in two ways. The first would be indentation on an exposed surface during the charging operation. The second would first complete the charging procedure and then perform immediate indentation on a region of tolerable homogeneity to obtain proper indentation results. This should reduce the amount of hydrogen escaping the microstructure before indentation is performed. Other work that has been considered revolves around using materials of different crystal structures specifically face-centered cubic (FCC) and hexagonal close packed (HCP) materials that have shown susceptibility to hydrogen. As a further extension to this, materials with precipitates that can act as trapping sites are another avenue upon which to explore as this work did not provide a quantification for a structure with a considerable amount of precipitates.

Thus, for applications that require a steel to be exposed to a hydrogen rich environment for durations greater than 24 hours, 1018 will prove to be better suited for the application than 4340 which will degrade beyond that time frame. While the stronger material when in air, 4340 suffers corrosion susceptibility that may reduce its usefulness in applications such as pressure vessels and pipelines. This can prove particularly problematic when the material is employed in automotive applications as the steel may be

exposed to hydrogen rich environments slightly over a long period of time. While this work does not encapsulate cyclic exposure to hydrogen rich environments, the next extension of the work here is to further extrapolate on the effects of slight hydrogen exposure over long periods of time. An extension of this work would also explore the time upon which 1018 does begin to exhibit similar corrosive degradation as 4340. Further analysis on 1018 would allow a more comprehensive evaluation of the properties that determine suitable for long exposure applications. This can help provide an accurate determination about the safety conditions for the cyclic use of a steel in corrosive environments.

REFERENCES

[1] W.H. Johnson, On some remarkable changes produced in iron and steel by the action of hydrogen and acids, Nature 11(281) (1875) 393.

[2] J. Venezuela, Q. Liu, M. Zhang, Q. Zhou, A. Atrens, The influence of hydrogen on the mechanical and fracture properties of some martensitic advanced high strength steels studied using the linearly increasing stress test, Corrosion Science 99 (2015) 98-117.

[3] F. Liu, Y. Zhao, Effects of hydrogen induced delay fracture on high-strength steel plate of automobile and the improvement, Frattura ed Integrità Strutturale 36 (2016) 139-150.

[4] Y. Kim, Y.J. Chao, M.J. Pechersky, M.J. Morgan, On the Effect of Hydrogen on the Fracture Toughness of Steel, International Journal of Fracture 134(3-4) (2005) 339-347.

[5] J. Ciruna, H. Szieleit, The effect of hydrogen on the rolling contact fatigue life of AISI 52100 and 440C steel balls, Wear 24(1) (1973) 107-118.

[6] H.J. Grabke, E. Riecke, Absorption and Diffusion of Hydrogen in Steels, Mater. Technol 34(6) (2000) 331-342.

[7] K. Takai, R. Watanuki, Hydrogen in trapping states innocuous to environmental degradation of high-strength steels, ISIJ International 43(4) (2003) 520-526.

[8] W.D. Callister Jr, D.G. Rethwisch, Fundamentals of Materials Science and Engineering: An Integrated Approach, John Wiley & Sons 2012.

[9] Y. Zhao, D.-H. Lee, M.-Y. Seok, J.-A. Lee, M.P. Phaniraj, J.-Y. Suh, H.-Y. Ha, J.-Y. Kim, U. Ramamurty, J.-i. Jang, Resistance of CoCrFeMnNi high-entropy alloy to gaseous hydrogen embrittlement, Scripta Materialia 135 (2017) 54-58.

[10] R.A. Oriani, The diffusion and trapping of hydrogen in steel, Acta Metallurgica 18(1) (1970) 147-157.

[11] P. Lang, M. Rath, E. Kozeschnik, P.E.J. Rivera-Diaz-del-Castillo, Modelling the influence of austenitisation temperature on hydrogen trapping in Nb containing martensitic steels, Scripta Materialia 101 (2015) 60-63.

[12] M. Aucouturier, Grain Boundary Segregations and Hydrogen Embrittlement, Le Journal de Physique Colloques 43 (C6) (1982) C6-175-C6-186.

[13] T. Depover, E. Wallaert, K. Verbeken, On the synergy of diffusible hydrogen content and hydrogen diffusivity in the mechanical degradation of laboratory cast Fe-C alloys, Materials Science and Engineering: A 664 (2016) 195-205.

[14] I. Robertson, H. Birnbaum, P. Sofronis, Hydrogen effects on plasticity, Dislocations in Solids 15 (2009) 249-293.

[15] A. Latifi V, R. Miresmaeili, A. Abdollah-Zadeh, The mutual effects of hydrogen and microstructure on hardness and impact energy of SMA welds in X65 steel, Materials Science and Engineering: A 679 (2017) 87-94.

[16] T. Neeraj, R. Srinivasan, J. Li, Hydrogen embrittlement of ferritic steels: Observations on deformation microstructure, nanoscale dimples and failure by nanovoiding, Acta Materialia 60(13-14) (2012) 5160-5171.

[17] J. Lufrano, P. Sofronis, H. Birnbaum, Modeling of hydrogen transport and elastically accommodated hydride formation near a crack tip, Journal of the Mechanics and Physics of Solids 44(2) (1996) 179-205.

[18] J. Lufrano, P. Sofronis, H. Birnbaum, Elastoplastically accommodated hydride formation and embrittlement, Journal of the Mechanics and Physics of Solids 46(9) (1998) 1497-1520.

[19] M. Smialowski, Hydrogen in steel: effect of hydrogen on iron and steel during production, fabrication, and use, Elsevier 2014.

[20] S. Thomas, N. Ott, R.F. Schaller, J.A. Yuwono, P. Volovitch, G. Sundararajan, N.V. Medhekar, K. Ogle, J.R. Scully, N. Birbilis, The effect of absorbed hydrogen on the dissolution of steel, Heliyon 2(12) (2016) e00209.

[21] S.J. Kim, K.Y. Kim, Hydrogen permeation in high strength steel under load in aqueous environment, Corrosion Engineering, Science and Technology 49(2) (2014) 136-142.

[22] M. Devanathan, Z. Stachurski, The adsorption and diffusion of electrolytic hydrogen in palladium, Proceedings of the Royal Society of London A: Mathematical, Physical and Engineering Sciences, The Royal Society, 1962, pp. 90-102.

[23] P. Novak, R. Yuan, B.P. Somerday, P. Sofronis, R.O. Ritchie, A statistical, physical-based, micro-mechanical model of hydrogen-induced intergranular fracture in steel, Journal of the Mechanics and Physics of Solids 58(2) (2010) 206-226.

[24] M.H. Sk, R.A. Overfelt, A.M. Abdullah, Effects of microstructures on hydrogen induced cracking of electrochemically hydrogenated double notched tensile sample of 4340 steel, Materials Science and Engineering: A 659 (2016) 242-255.

[25] I.-O. Shim, J. Byrne, A study of hydrogen embrittlement in 4340 steel I: Mechanical aspects, Materials Science and Engineering: A 123(2) (1990) 169-180.

[26] A. Laureys, T. Depover, R. Petrov, K. Verbeken, Microstructural characterization of hydrogen induced cracking in TRIP-assisted steel by EBSD, Materials Characterization 112 (2016) 169-179.

[27] A. McNabb, P. Foster, A new analysis of the diffusion of hydrogen in iron and ferritic steels, Trans. Metall. Soc. AIME 227(3) (1963) 618-627.

[28] A. Turnbull, R.B. Hutchings, D.H. Ferriss, Modelling of thermal desorption of hydrogen from metals, Materials Science and Engineering A238 (1997) 317-328.

[29] M.P. Puls, Elastic interactions of hydrogen in the lattice of iron alloys, Hydrogen Degradation of Ferrous Alloys 114-130.

[30] C. Hwang, I. Bernstein, Dislocation transport of hydrogen in iron single crystals, Acta Metallurgica 34(6) (1986) 1001-1010.

[31] J.P. Hirth, Effects of hydrogen on the properties of iron and steel, Metallurgical Transactions A 11(6) (1980) 861-890.

[32] J. Takahashi, K. Kawakami, Y. Kobayashi, T. Tarui, The first direct observation of hydrogen trapping sites in TiC precipitation-hardening steel through atom probe tomography, Scripta Materialia 63(3) (2010) 261-264.

[33] G. Pressouyre, Trap theory of hydrogen embrittlement, Acta Metallurgica 28(7) (1980) 895-911.

[34] K. Takai, H. Shoda, Dynamic behavior of hydrogen desorption from pure iron and inconel 625 during elastic and plastic deformations, Revista Materia 15(2) (2010) 267-274.

[35] S. Evers, T. Hickel, M. Koyama, R. Nazarov, M. Rohwerder, J. Neugebauer, D. Raabe, M. Stratmann, Microstructure effects on hydrogen embrittlement in austenitic steels: a multidisciplinary investigation (2016).

[36] J. Toribio, D. Vergara, M. Lorenzo, Influence of loading rate on the hydrogen-assisted micro-damage in bluntly notched samples of pearlitic steel, Metals 6(1) (2016) 11.

[37] X. Du, W. Cao, C. Wang, S. Li, J. Zhao, Y. Sun, Effect of microstructures and inclusions on hydrogen-induced cracking and blistering of A537 steel, Materials Science and Engineering: A 642 (2015) 181-186.

[38] M.N. Inés, C.A. Asmus, G.A. Mansilla, Influence of total strain amplitude on hydrogen embrittlement of high strength steel, Procedia Materials Science 8 (2015) 1039-1046.

[39] A. Shibata, T. Murata, H. Takahashi, T. Matsuoka, N. Tsuji, Characterization of hydrogen-related fracture behavior in as-quenched low-carbon martensitic steel and tempered medium-carbon martensitic steel, Metallurgical and Materials Transactions A 46(12) (2015) 5685-5696.

[40] M. Koyama, E. Akiyama, T. Sawaguchi, D. Raabe, K. Tsuzaki, Hydrogen-induced cracking at grain and twin boundaries in an Fe–Mn–C austenitic steel, Scripta Materialia 66(7) (2012) 459-462.

[41] N. Eliaz, A. Shachar, B. Tal, D. Eliezer, Characteristics of hydrogen embrittlement stress corrosion cracking and tempered martensite embrittlement in high-strength steels, Engineering Failure Analysis 9 (2000) 167-184.

[42] N. Winzer, O. Rott, R. Thiessen, I. Thomas, K. Mraczek, T. Höche, L. Wright, M. Mrovec, Hydrogen diffusion and trapping in Ti-modified advanced high strength steels, Materials & Design 92 (2016) 450-461.

[43] Z. Cui, Z. Liu, L. Wang, X. Li, C. Du, X. Wang, Effect of plastic deformation on the electrochemical and stress corrosion cracking behavior of X70 steel in near-neutral pH environment, Materials Science and Engineering: A 677 (2016) 259-273.

[44] G. Olson, Brains of steel: designing materiallurgists, Advanced Materials Processes 152(1) (1997) 72-79.

[45] L.M. Dougherty, E.K. Cerreta, E.A. Pfeif, C.P. Trujillo, G.T. Gray, The impact of peak shock stress on the microstructure and shear behavior of 1018 steel, Acta Materialia 55(18) (2007) 6356-6364.

[46] M.D. Danford, The role of grain boundaries in hydrogen diffusion in metals at 25 C, NASA Technical Memorandum 108407 (1993).

[47] K.-i. Takai, Y. Chiba, K. Noguchi, A. Nozue, Visualization of the hydrogen desorption process from ferrite, pearlite, and graphite by secondary ion mass spectrometry, Metallurgical and Materials Transactions A 33(8) (2002) 2659-2665.

[48] S. Chan, J. Charles, Effect of carbon content on hydrogen occlusivity and embrittlement of ferrite–pearlite steels, Materials Science and Technology 2(9) (1986) 956-962.

[49] H.-L. Lee, S.L.-I. Chan, Hydrogen embrittlement of AISI 4130 steel with an alternate ferrite/pearlite banded structure, Materials Science and Engineering: A 142(2) (1991) 193-201.

[50] A. Handbook, Corrosion of Titanium and Titanium Alloys, 13 675.

[51] D.P. Escobar, T. Depover, L. Duprez, K. Verbeken, M. Verhaege, Combined thermal desorption spectroscopy, differential scanning calorimetry, scanning electron microscopy and x-ray diffraction study of hydrogen trapping in cold deformed TRIP steel, Acta Materialia 60(6) (2012) 2593-2605.

[52] H.K. Birnbaum, P. Sofronis, Hydrogen-enhanced localized plasticity - a mecanism for hydrogen-related fracture, Materials Science and Engineering A176 (1994) 191-202.

[53] P. Sofronis, R.M. McMeeking, Numerical analysis of hydrogen transport near a blunting crack tip, J. Mech. Phys. Solids. 37(3) (1989) 317-350.

[54] S. Frappart, X. Feaugas, J. Creus, F. Thebault, L. Delattre, H. Marchebois, Hydrogen solubility, diffusivity and trapping in a tempered Fe–C–Cr martensitic steel under various mechanical stress states, Materials Science and Engineering: A 534 (2012) 384-393.

[55] A. Oudriss, J. Creus, J. Bouhattate, E. Conforto, C. Berziou, C. Savall, X. Feaugas, Grain size and grain-boundary effects on diffusion and trapping of hydrogen in pure nickel, Acta Materialia 60(19) (2012) 6814-6828.

[56] T. Doshida, K. Takai, Dependence of hydrogen-induced lattice defects and hydrogen embrittlement of cold-drawn pearlitic steels on hydrogen trap state, temperature, strain rate and hydrogen content, Acta Materialia 79 (2014) 93-107.

[57] E.I. Galindo-Nava, B.I.Y. Basha, P.E.J. Rivera-Diax-del-Castillo, Hydrogen transport in metlas: Integration of permeation, thermal desorption and degassing, (2016).

[58] D. Johnson, J. Wu, Hydrogen transport in carbon steels as a function of carbon content and heat treatment near 298 K, Journal of Materials for Energy Systems 8(4) (1987) 402-408.

[59] E. Legrand, J. Bouhattate, X. Feaugas, H. Garmestani, Computational analysis of geometrical factors affecting experimental data extracted from hydrogen permeation tests: II–consequences of trapping and an oxide layer, International Journal of Hydrogen Energy 37(18) (2012) 13574-13582.

[60] E. Legrand, A. Oudriss, S. Frappart, J. Creus, X. Feaugas, J. Bouhattate, Computational analysis of geometrical factors affecting experimental data extracted from hydrogen permeation tests: III–Comparison with experimental results from the literature, International Journal of Hydrogen Energy 39(2) (2014) 1145-1155.

[61] K. Kawakami, T. Matsumiya, Numerical analysis of hydrogen trap state by TiC and V4C3 in bcc-Fe, ISIJ international 52(9) (2012) 1693-1697.

[62] W. Choo, Effect of cathodic charging current density on the apparent hydrogen diffusivity through pure iron, Journal of Materials Science 19(8) (1984) 2633-2638.

[63] S. Frappart, X. Feaugas, J. Creus, F. Thebault, L. Delattre, H. Marchebois, Study of the hydrogen diffusion and segregation into Fe–C–Mo martensitic HSLA steel using electrochemical permeation test, Journal of Physics and Chemistry of Solids 71(10) (2010) 1467-1479.

[64] J. Wu, Electrochemical method for studying hydrogen in iron, nickel and palladium, International Journal of Hydrogen Energy 17(12) (1992) 917-921.

[65] S.-M. Lee, J.-Y. Lee, The trapping and transport phenomena of hydrogen in nickel, Metallurgical and Materials Transactions A 17(2) (1986) 181-187.

[66] S.M. Charca, O.N. Uwakweh, V.S. Agarwala, Hydrogen transport conditions and effects in cathodically polarized AF1410 steel, Metallurgical and Materials Transactions A 38(10) (2007) 2389-2399.

[67] L. Tau, S.L.I. Chan, Effects of ferrite/pearlite alignment on the hydrogen permeation in a AISI 4130 steel, Materials Letters 29 (1996) 143-147.

[68] E.J. Song, D.-W. Suh, H. Bhadeshia, Theory for hydrogen desorption in ferritic steel, Computational Materials Science 79 (2013) 36-44.

[69] J.S. Kim, Y.H. Lee, D.L. Lee, K.-T. Park, C.S. Lee, Microstructural influences on hydrogen delayed fracture of high strength steels, Materials Science and Engineering: A 505(1) (2009) 105-110.

[70] F. Fischer, J. Svoboda, E. Kozeschnik, Interstitial diffusion in systems with multiple sorts of traps, Modelling and Simulation in Materials Science and Engineering 21(2) (2013) 025008.